DEVELOPMENT OF A LABEL-FREE ELECTROCHEMICAL DNA BIOSENSOR FOR THE MODEL ANALYTE OF BREAST CANCER RELATED SEQUENCES

A thesis submitted as a partial requirement for the degree of
Master of Research

Benjamin Richard Pendleton
Bachelor of Science (Chemistry)

October 10, 2014

Macquarie University
Faculty of Science
Department of Chemistry and Biomolecular Sciences

ACKNOWLEDGEMENTS

Firstly I would like to thank my supervisor, Dr Danny Wong, for continued advice, guidance and encouragement throughout the duration of this work. I would like to thank the Chemistry and Biomolecular Sciences, Master of Research Academic Committee for their administrational excellence throughout the program. I would like to thank the chemistry teaching laboratory technicians for providing me with work space during an unforeseen laboratory closure in the department. I would also like to thank my fellow members of the Electroanalytical Chemistry Research Group, Md Mominul Haque, Shajahan Siraj and Thomas Somerville for providing knowledgeable insights, introducing research facilities and for friendship throughout my candidature. To members of my cohort, thank you for making the journey enjoyable and rewarding. Finally, I would like to thank my friends and family for their unconditional support and encouragement and who were paramount in maintaining a sustainable and productive work-life balance.

ABSTRACT

In this work, a label-free electrochemical DNA biosensor capable of detecting a single-mismatch in a breast cancer gene 1 *(BRCA1)* related sequence was developed. Single nucleotide polymorphisms in the *BRCA1* tumour suppressing gene have been reported to cause breast cancer, a genetic-based disease that is one of the leading causes of mortality worldwide. The label-free biosensor platform consisted of graphene, a phenyl linker and gold nanoparticles, immobilised on a glassy carbon electrode. To this anchoring layer, a 19 mer, thiol-labelled DNA probe was covalently attached, followed by hybridisation with its complementary target, a *BRCA1* related DNA sequence, and finally zirconium was incorporated into the DNA duplex for electrochemical signal amplification. In this work, a two-level factorial design was used for optimisation of the significant factors and their interactions in biosensor performance. The change in oxidation current of ferrocenecarboxylic acid following hybridisation was used to voltammetrically study the analytical performance of the biosensor. Using square wave voltammetry, a linear dynamic range between 15.5 and 100 nM of the DNA target, with a detection limit of 4.6 nM and reproducibility of 4% was achieved.

TABLE OF CONTENTS

Chapter 1: Introduction

1.1 Introduction to deoxyribonucleic acid hybridisation 1
1.2 Electrochemical DNA biosensors 2
1.2.1 Application of electrochemical DNA biosensors to detection of genetic mutations 4
1.2.2 Use of nanomaterials in biosensing 5
1.2.3 Immobilisation of biorecognition element 8
1.2.4 Electrochemical DNA biosensor hybridisation detection techniques 9
1.3 Scope of present study 12

Chapter 2: Experimental

2.1 Introduction 14
2.2 Reagents 14
2.3 Electrochemical instrumentation 16
2.4 Electrode preparation 17
2.5 Fabrication of glassy carbon electrode sensing platform 17
2.5.1 Preparation of graphite oxide 17
2.5.2 Preparation of graphene oxide 18
2.5.3 Immobilisation of graphene on glassy carbon electrodes 18
2.5.4 ERGO-glassy carbon electrode surface modification with *in situ* generated aryl diazonium cations 18
2.5.5 Gold nanoparticle modified electrode 18
2.6 Detection of DNA hybridisation 19
2.7 Characterisation of graphite oxide 20
2.8 Statistical analysis 20

Chapter 3: Results and Discussion

3.1 Introduction 21
3.2 Preparation of bare glassy carbon electrodes 22
3.3 Fabrication of biosensing platform 22
3.3.1 Immobilisation of graphene on glassy carbon electrodes 22
3.3.2 ERGO-glassy carbon surface modification with *in situ* generated aryl diazonium cations 25
3.3.3 Gold nanoparticle modified electrode surface 27
3.3.4 Factorial design optimisation 29
3.4 Detection of DNA hybridisation 39

Chapter 4: Conclusion

4.1 Concluding remarks 46
4.2 Future directions 48

Chapter 5: References

5.1 Reference list 50

Chapter 6: Supplementary Material

6.1 Supplementary material 53

LIST OF ABBREVIATIONS

A	adenine
ATR	attenuated total reflectance
AuNP	gold nanoparticle
C	cytosine
DNA	deoxyribonucleic acid
dsDNA	double-stranded DNA
EDTA	ethylenediaminetetraacetic acid
EIS	electrochemical impedance spectroscopy
ERGO	electrochemically reduced graphene oxide
$Fe(CN)_6^{3-/4-}$	ferricyanide-ferrocyanide redox marker
FTIR	fourier transform infrared
G	guanine
PBS	phosphate-buffered saline
Ph	4-phenyl
R_{et}	electron transfer resistance
R_s	solution resistance
$Ru(NH_4)_6^{3+/2+}$	ruthenium(III) hexaammine redox marker
SNP	single nucleotide polymorphism
ssDNA	single-stranded DNA
T	thymine
TCEP	tris-(2-carboxyethyl)phosphine hydrochloride
TE	tris-ethylenediaminetetraacetic acid
Z_w	Warburg impedance
Zr(IV)	zirconium(IV)

Chapter 1

INTRODUCTION

1.1 Introduction to deoxyribonucleic acid hybridisation

Hybridisation between deoxyribonucleic acid (DNA) sequences is a fundamental process of molecular biology and detection of hybridisation events is the foundation of many analytical applications. Hybridisation occurs through Watson-Crick base pairing, resulting from hydrogen bonding between complementary purines (adenine (A) and guanine (G)) and pyrimidines (cytosine (C) and thymine (T)). More specifically, base pairing occurs through hydrogen bonding (i) between A and T, and (ii) between C and G.[1-3] Hybridisation of complementary nucleotides is shown in Figure 1.1, which depicts the nucleotide structure and intermolecular hydrogen bonding of AT and CG complementary bases. Hybridisation is detected in this figure, with AT and CG hybridisation occurring through formation of a double hydrogen bond and triple hydrogen bond, respectively. Consequently, CG complexes exhibit a superior bond strength than AT duplexes due to the nature of the stronger, triple hydrogen bond.[2,3]

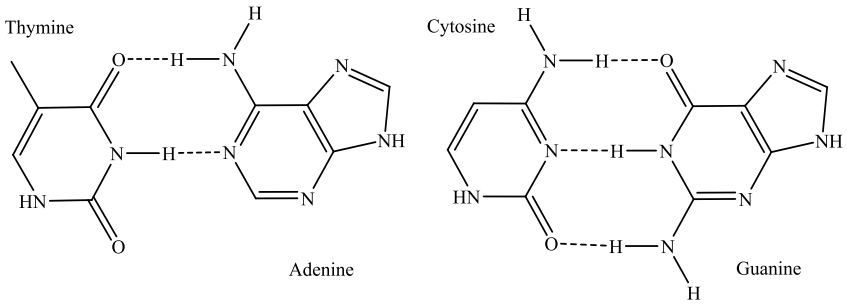

Figure 1.1 DNA base pairing between complementary DNA nucleotides (AT and CG) through hydrogen bonding. Hydrogen bonding between nucleotide bases is depicted by dashed lines.

The detection of sequence-specific DNA, through monitoring of hybridisation, has generated high interest due to the ability to perform analytical detection for a range of applications including monitoring of the effectiveness of pharmaceutical agents,[4] forensic-based

applications,[5] environmental analysis[6] and pathogen detection.[7,8] In these applications, DNA hybridisation has been traditionally performed by techniques including colourimetric and enzyme-based assays,[9] gel electrophoresis-based techniques[10,11] and polymerase chain reaction.[12] For example, DNA hybridisation, through the use of polymerase chain reaction and *in situ* DNA hybridisation, was performed to detect salmonella in water, faeces and fish intestines for environmental monitoring applications.[6] More specifically, hybridisation of sample DNA sequences immobilised on a slide with a fluorescent probe, specific for salmonella DNA sequences, was detected by microscopy following successful hybridisation. Despite these traditional methods being effective for the monitoring of DNA hybridisation, they are time consuming, labour intensive and required equipment is generally non-portable.[8,13-16] This has prompted development of newer, faster, more portable and simpler analytical techniques to replace traditionally used assays to detect DNA hybridisation.

1.2 Electrochemical DNA biosensors

The concept of biosensors and the monitoring of DNA hybridisation can be coupled with electrochemistry to yield electrochemical DNA biosensors.[13,14,17,18] Biosensors are devices that incorporate a biological recognition element with a transducing element to quantitatively determine the concentration of a range of target analytes. The biological recognition element imparts selective analytical detection and the transducer converts the biological recognition element into a measurable signal.[8,19] Since the development of the first enzyme biosensor by Clark and Lyons in 1962 using an enzyme biological recognition element,[20] a range of other biological sensing elements have been incorporated in biosensors including antibodies,[21-23] enzymes[15,24] and nucleic acids,[8,13,17,25] to impart specific detection selectivity for the analysis of a range of target biological analytes. While different biological sensing elements are useful in the detection of specific biological analytes in biosensors, the incorporation of nucleic acids as the biosensing element to facilitate detection is the focus of this work.

DNA can be used as the biological recognition element in electrochemical biosensors to facilitate the detection of DNA hybridisation. The basis of electrochemical DNA biosensors involves immobilisation of a single-stranded DNA (ssDNA) probe on a substrate surface and subsequent hybridisation with a complementary sequence to form a double-stranded DNA (dsDNA) duplex.[13,14,19] By incorporating an electrochemical transducing element as the substrate surface to which the biological element is immobilised, for example an electrode, the current response following hybridisation can be detected. The electrochemical detection

of DNA hybridisation is depicted in Figure 1.2. In this figure, a probe ssDNA sequence is attached to an electrode transducing element, and upon hybridisation with a target ssDNA, the formation of hybridised dsDNA occurs. A net change in electrochemical response can be observed during the hybridisation event through the use of label or label-free approaches, including (i) labelling with electroactive species,[26] (ii) label-free redox markers[13] and more recently, (iii) the direct monitoring of intrinsic A and G oxidation.[27] This concept of monitoring hybridisation using electrochemical DNA biosensors and the three common electrochemical approaches to detection will be further discussed in Section 1.2.4.

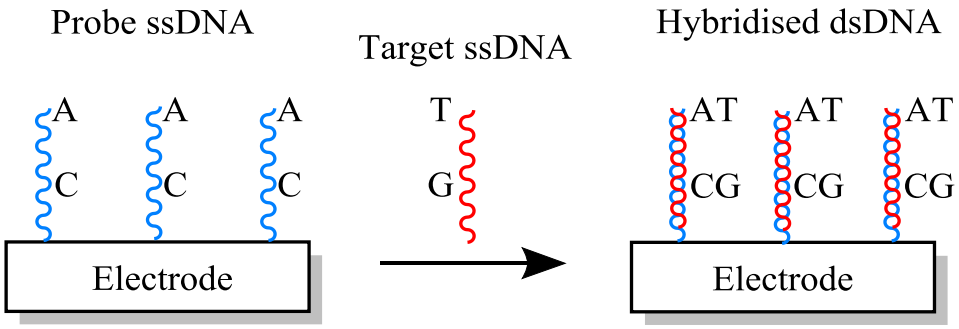

Figure 1.2 Hybridisation event of an ssDNA probe sequence immobilised on an electrode transducing surface and hybridisation with a complementary ssDNA target sequence to form a dsDNA duplex. The degree of hybridisation can be monitored using an array of electroanalytical techniques.

Electrochemical DNA biosensors are advantageous over other biosensing systems and traditional methods of hybridisation detection due to the feasibility of miniaturisation, portability, sensitivity, simplicity of analysis and the economic nature of DNA biosensors.[14,18,19] As a result of these excellent properties, electrochemical DNA biosensors exhibit great potential for medical applications in point-of-care disease diagnostics for the identification of mutations at the genomic level and to facilitate the possibility of future, personalised diagnostics.[14,28,29] The detection of genetic mutations through the use of electrochemical DNA biosensors to monitor DNA hybridisation has been reported.[14,28,30] Applications of electrochemical DNA biosensors and strategies to improving the performance of electrochemical DNA biosensors are subsequently outlined.

1.2.1 Application of electrochemical DNA biosensors to detection of genetic mutations

Genetic mutations are responsible for a number of genetically inherited conditions and diseases and contribute enormous costs to global healthcare systems.[18,31] Single nucleotide polymorphisms (SNPs) are a genetically inherited condition responsible for a range of genetic-based diseases including cystic fibrosis and breast cancer.[1,28] Electrochemical DNA biosensors demonstrated great potential for medical applications in point-of-care disease diagnostics for the identification of mutations at the genomic level, including SNPs and to facilitate the possibility of future, personalised diagnostics.[14,28,29] Detection of genetic mutations can therefore be performed through the use of electrochemical DNA biosensors to monitor DNA hybridisation.[14,28,30]

Breast cancer, a disease caused by SNPs, is one of the leading causes of mortality worldwide.[14] The disease is often caused by a range of mutations in the tumour suppressing gene, *BRCA1*, which introduces stop codons resulting in the loss of protein function.[1,14,30,31] An example of the introduction of stop codons is shown in Figure 1.3, which shows a *BRCA1* target sequence based on E908X WT breast cancer 1.[1] Figure 1.3 also shows the effect that polymorphisms can impart on protein functionality through the introduction of stop codons in both the SNP and three-base mismatch DNA sequences. In this figure, possible gene mutations are underlined and contain different DNA sequences to the target sequence. The mutation of DNA sequence can potentially lead to the introduction of stop codons in the DNA sequence and an example of introduced stop codons is shown in Figure 1.3 with the sequence depicted in pink. Early detection of cancerous growth is critical in improving survival rate of the disease, however current detection methods generally only provide diagnostic confirmation at latter stages of cancerous growth.[14] As a result of the nature and importance of *BRCA1* mutations, related DNA sequences are ideal candidates for biological recognition elements in electrochemical DNA biosensors.

BRCA1 target sequence:	GAA CAA AAG GAA GAA AAT C
BRCA1 SNP sequence:	GAA CAA AAG GAA **T**AA AAT C
BRCA1 three-base mismatched sequence:	GAA CAA ATC **T**AA GAA AAT C

Figure 1.3 ssDNA sequences relating to *BRCA1* gene based on E908X WT breast cancer 1 target sequence for *in vitro* detection using electrochemical DNA biosensors.[1] All DNA sequences are presented 5' to 3', mutated bases are underlined and introduced stop codons are shown in pink.

A number of DNA biosensors for detection of *BRCA1* sequences have been reported. A *BRCA1* biosensor based on the use of DNA modified with streptavidin coated paramagnetic beads, magnetic graphite composite electrodes and the electrochemical detection of gold tags was developed.[28] The reported DNA biosensor displayed a detection limit of 0.7 μM of the complementary *BRCA1* related gene sequence target, displayed in Figure 1.3. Mohan *et al.*[14] developed a *BRCA1* targeting biosensor incorporating a carboxyindole conducting polymer modified glassy carbon electrode, with electrochemical detection of intrinsic oxidation by electrochemical impedance spectroscopy (EIS). The biosensor exhibited an excellent detection limit of 0.01 fM of the complementary *BRCA1* related gene sequence target in Figure 1.3. Li *et al.*[1] also reported an electrochemical biosensor for the detection of the target *BRCA1* gene sequence on a carbon nanotube modified screen printed electrode with a detection limit of 0.4 μM. However despite the higher detection limit, the biosensor was reported to be more simplistic in nature, more cost effective and more reproducible results were obtainable in shorter time periods than other developed *BRCA1* biosensors.[1] In addition to biosensors displaying a low detection limit, these biosensor attributes are also of important consideration when designing a DNA biosensor with potential commercial applications. The nature of genetic mutations warrants further research into development of sensitive, selective and effective electrochemical DNA biosensors for detection and early diagnostics, which could potentially be achieved through the incorporation of nanomaterials in the biosensor design, immobilisation strategy of DNA biological sensing elements and electrochemical detection technique utilised for detection of the hybridisation phenomenon.

1.2.2 Use of nanomaterials in biosensing

The modification of electrochemical DNA biosensors with nanomaterials has recently been widely reported.[13,22,29,32] Nanomaterials have been reported in the modification of transducing surface, to which a biorecognition element is immobilised. A diverse range of nanomaterials including carbon nanofibres,[13] carbon nanotubes,[1] nanodiamonds,[22,33] graphene,[18,32,34] gold nanoparticles[35,36] and nanocomposite materials,[24,29] have been reported to modify the transducer surface in fabricated DNA biosensor designs. These nanomaterials have been incorporated in biosensor designs to increase the sensitivity of the biosensor, through enhancement of the surface area and conductivity of the biosensor transducing element, and to impart selective detection through facilitating attachment of biological recognition species.[13,29,30] Additionally nanomaterials have been exploited in biosensors to amplify the electrochemical detection signal.[13,28,37]

Among these nanomaterials, graphene first isolated in 2004,[38] exhibits a two-dimensional lattice of sp^2 carbon atoms with delocalised π orbitals. Graphene displays a large surface area, fast electron transfer, facilitates high electrical conductivity due to π electron charge transfer and can be produced at relatively low cost.[30,32,39,40] Graphene can be produced by a number of techniques including chemical vapour deposition, graphite exfoliation and reduction of graphene oxide through chemical, electrochemical and thermal reduction.[39] Of these synthetic methods, electrochemical reduction is an effective, simple and green approach to reduction of graphene oxide,[32,39] which can be prepared by reacting graphite with strong oxidising agents following the Hummers[41] and Staudenmaier methods.[42] As a result of the favourable properties to electrochemical applications, and ease of production, graphene was used in the development of a range of electrochemical DNA biosensors.

Graphene has been incorporated in electrochemical DNA biosensors to increase the surface area, and more importantly enhance electrical conductivity, of the transducing element, with picomolar detection limits of complementary target oligonucleotide sequences reported for some graphene-based sensors.[32,34] As a result, graphene has been utilised in a number of applications including the modification of transducing elements with graphene[32,34,35] and nanocomposite materials[35,43] to enhance sensitivity, and to facilitate the attachment of DNA oligonucleotides to graphene.[18,30] By incorporating graphene in the development of electrochemical sensor scaffolds with multiple nanomaterials, known as nanocomposites, the unique features of all constituents will complement each other and synergistically contribute to the targeted analytical properties, for example, benefits of different nanoparticle modified glassy carbon electrodes were observed to enhance the detection sensitivity in detection of the $Fe(CN)_6^{3-/4-}$ redox couple.[35] This dual nanomaterial scaffold showed superior sensitivity over a graphene-only design due to enhanced charge transfer between the nanoparticles and the glassy carbon electrode. The precursor to reduced graphene, graphene oxide, has also been incorporated in electrochemical DNA biosensors designs.[29,44,45] While not providing substantially enhanced conductivity, graphene oxide exhibits high surface area, stability, offers potential for modification of surface oxygen groups and has also been demonstrated to catalyse cleavage of proteins.[45]

Gold nanoparticles are another nanomaterial that offers a range of beneficial properties for electrochemical DNA biosensors including a high surface-area-to-volume ratio, good biocompatibility, high stability and the ability to facilitate electron transfer between a

biorecognition element and an electrode.[35,36,46] Gold nanoparticles can be prepared using a number of synthetic pathways including chemical reduction[36,46] and electrochemical reduction[35,47] of chloroauric acid ($HAuCl_4$), and recently a "green chemistry" approach using the gripe water reduction method.[48] The size of gold nanoparticles is a distinguishing factor of nanoparticles from the bulk material and is a critical consideration in electrode modification. In applications of gold nanoparticles to electrochemical biosensing, a compromise is required between the surface area of modified electrode surfaces, depending on the size of nanoparticles, and selectivity of the sensor to the specific applications.[47] Gold nanoparticles have been incorporated into electrochemical transducer frameworks of electrochemical DNA biosensors reported in a number of studies,[35,43] to increase the surface area of the electrode and enhance the measurable peak currents generated by an electroactive compound and to facilitate selective analyte detection.

Despite the advantageous properties of gold nanoparticles for DNA biosensing, the use of gold nanoparticles is associated with some limitations including potential agglomeration of synthesised gold nanoparticles and the stability of the sensing interface.[36,47] Uniform distribution of gold nanoparticles can be facilitated by incorporating amine groups that provide potential sites for bonding to synthesised gold nanoparticles.[35] However, the use of NH-Au bonds to incorporate gold nanoparticles in biosensing applications is limited due to the relatively poor stability of the covalent NH-Au bond (of bond strength 154 kJ mol^{-1}).[36] A recent approach to increase the stability of gold nanoparticle modified interfaces was to utilise the stronger gold-carbide bond of bond strength 317 kJ mol^{-1} for the attachment of gold nanoparticles.[36] In this approach, gold nanoparticles were incorporated on an amine modified glassy carbon electrode by diazonium chemistry and electrochemical reduction in a solution containing gold nanoparticles.[36] The fabricated gold nanoparticle modified electrode, with C-Au bonds, was reported to be significantly more stable than the corresponding electrode containing NH-Au bonds to facilitate the covalent attachment of gold nanoparticles. Therefore in biosensing applications, the addition of gold nanoparticles through C-Au bonds is a promising approach to utilising the advantageous properties of gold nanoparticles while maintaining electrode platform stability.

Zirconium, the inorganic ion Zr(IV), is a species with low system toxicity and a strong affinity for oxygen containing functional groups.[13,33] This species has strong potential for use in DNA biosensor applications as Zr(IV) can coordinate within the negatively charged

phosphate groups of DNA duplexes and attract a range of oxygen containing compounds. Zr(IV) is particularly attractive for biosensing applications as it can be directly incorporated into the transducing framework and it can also be used in applications following the DNA hybridisation event to amplify the detection signal. Liu *et al.*[33] reported an electrochemical DNA biosensor with a thin zirconia layer which was used to anchor a DNA oligonucleotide probe to a diamond electrode surface. The electrode design included electrochemical deposited zirconia layers on diamond electrode transducing surfaces to facilitate the immobilisation of ssDNA probes sequences with incorporated oxygen-containing phosphate labels. Our laboratory has previously reported a DNA biosensor based on a carbon-nanofibre, chitosan and glutaraldehyde anchoring framework with the addition of Zr(IV) ions to the DNA modified sensors.[13] Zirconia was incorporated in the reported design to coordinate with the negatively charged phosphate backbone of hybridised DNA to attract an oxygen-containing redox marker, ferrocenecarboxylic acid, to the biosensor surface for highly sensitive, label-free detection.[13] However, the selectivity of this electrochemical DNA biosensor towards single-base mutations of a complementary target sequence was not demonstrated.

1.2.3 Immobilisation of biorecognition element

The method of biorecognition element immobilisation on a transducer surface is also an important consideration in electrochemical DNA biosensor development. Different approaches to the immobilisation strategy of DNA sequences have been reported and they contribute important properties to the overall performance of the biosensor. The immobilisation strategy of DNA sequences can directly affect the orientation of DNA probes with respect to the transducer surface,[49] surface coverage of ssDNA probe oligonucleotides[50] and the stability of the attachment of ssDNA probe sequences to the biosensor surface.[51] Both non-covalent and covalent bonding approaches have been used to immobilise DNA sequences on transducer surfaces.

Non-covalent immobilisation methods of ssDNA have been reported in a range of applications with specific transducer materials.[33,52-54] Kang *et al.*[52] reported the use of non-covalent ssDNA immobilisation to adsorb ssDNA to carbon nanotubes through π-π stacking in order to increase the dispersion of carbon nanotubes during modification of the transducing surface. As described previously, a zirconium layer attached to a diamond electrode, by electrochemical reduction, has been used to coordinate terminal phosphate labelled probe

ssDNA to a diamond electrode.[33] Another approach to non-covalent ssDNA probe immobilisation is to electrostatically attract an anionic ssDNA to a cationic copolymer modified surface.[53,54]

Meanwhile, ssDNA sequences can also be covalently attracted to an electrode surface. This approach utilising covalent bonding offers greater control of immobilisation and increased stability. For example, amine and carboxylic acid functionalised DNA probes are often covalently immobilised on a modified electrode surface.[13] Diazonium chemistry is another strategy for attaching the amine groups of an ssDNA probe to terminal grafted amino groups an electrode surface through the use of diazonium reactions and amine chemistry.[49] The affinity of thiols for gold (bond energy of S-Au bonds is 154 kJ mol^{-1})[36] is a popular approach to covalently immobilise probe sequences directly to a range of surfaces including bulk gold electrodes,[55] using self-assembling monolayers,[8] and also gold nanoparticles.[35]

1.2.4 Electrochemical DNA biosensor hybridisation detection techniques

Following the DNA hybridisation event, the performance of electrochemical DNA biosensors can be analytically determined using a range of electrochemical techniques. Commonly applied electrochemical techniques to the analysis of DNA biosensors include cyclic voltammetry,[13,29,56] differential pulse voltammetry,[13,28,49] square wave voltammetry[8,29,47] and EIS.[29,32,56] Each of these electrochemical techniques requires the detection of an electrochemically active species and can utilise either label or label-free approaches to facilitate the detection and quantitation of DNA hybridisation.

Label-based detection methods involve the addition of readily detectable molecules, often electroactive species, which can be used to indicate hybridisation efficiency. Labelled approaches can involve the incorporation of a redox active label in a DNA sequence and upon hybridisation with a complementary DNA probe, already immobilised on an electrode surface, the spatial proximity of the redox species and electrode changes and an increase in electrochemical signal is observed.[25,57] For example, Le Floch *et al.*[58] incorporated the electroactive ferrocene in a cationic polymer framework, so that it was attracted to negatively charged hybridised DNA. The probe was a neutral peptide nucleic acid sequence and upon hybridisation, the duplex exhibited a net negative charge. The quantity of ferrocene at the electrode surface, through electrostatic interactions between the electroactive cationic polymer and anionic DNA duplex, was therefore directly proportional to efficiency of the

hybridisation event. Alternatively, labelled approaches involving enzyme facilitated chemical reactions, producing electroactive compounds are also well documented.[59,60] Despite low sensitivities being achieved with labelled approaches, a number of disadvantages are identifiable including inefficiency of many labelling reactions, time requirement for labelling and the potential for manipulation of the properties of the biorecognition event, for example, through imparting steric hindrance with bulky electroactive labels.

Label-free hybridisation detection includes the use of electroactive markers and direct monitoring of the intrinsic oxidation of A and G purine nucleotides. Both of these label-free approaches offer advantages over the incorporation of electroactive labels, for detection of hybridisation in DNA biosensors, due to simplicity, the ability to perform real-time monitoring avoiding the requirement of labelling reactions and without the addition of labels which may potentially manipulate properties of the biorecognition element.[13,16]

Electroactive or redox markers rely on the change in electrochemical signal following hybridisation, which is affected by the transduction and biorecognition element in electrochemical DNA biosensors. Electroactive markers will undergo redox processes at a specific potential, giving rise to a measurable current. A number of research groups have used redox markers in label-free detection of DNA hybridisation to take advantage of the favourable properties of label-free hybridisation analysis.[13,17,32,61] One commonly reported application of label-free redox markers involves the use of the hexaammineruthenium(III) redox couple [$Ru(NH_3)_6^{3+/2+}$], shown in Equation 1.1, to quantitatively analyse the hybridisation efficiency of ssDNA sequences.[32,61] The positively charged $Ru(NH_3)_6^{3+/2+}$ redox couple was electrostatically attracted to the negatively charged dsDNA phosphate backbone to increase the generated signal at the electrode surface. Alternatively, electrostatic interactions between ssDNA/dsDNA on modified sensors and the negatively charged ferricyanide/ferrocyanide redox couple [$Fe(CN)_6^{3-/4-}$], shown in Equation 1.2 have been reported.[13,17] The DNA duplex exhibits a net negative charge as a result of the phosphate backbone, and electrochemical characterisation with a negatively charged redox marker results in electrostatic repulsion and reduced ability of the electroactive marker to undergo redox processes at the electrode surface, resulting in a decreased signal. Neutral redox markers, for example the ferrocenecarboxylic acid redox couple, shown in Equation 1.3, were used in a label-free method of detection through non-electrostatic interactions, for example to facilitate attraction to hybridised DNA through a zirconium-dsDNA framework.[13] In

applying these redox markers to label-free hybridisation detection, it is important to note that $Fe(CN)_6^{3-/4-}$ is an inner sphere redox marker strongly affected by surface modification and is more dependent on electrode surface functionality,[18,62] whereas both $Ru(NH_3)_6^{3+/2+}$ and ferrocenecarboxylic acid are outer sphere redox markers that are insensitive to surface chemistry and dependent on the distance between the redox marker and electrode surface.[62] Therefore the nature of redox marker is an important consideration in performing label-free electrochemical detection.

$$Ru(NH_3)_6^{3+} + e^- \leftrightarrow Ru(NH_3)_6^{2+} \qquad \textbf{Equation 1.1}$$

$$Fe(CN)_6^{3-} + e^- \leftrightarrow Fe(CN)_6^{4-} \qquad \textbf{Equation 1.2}$$

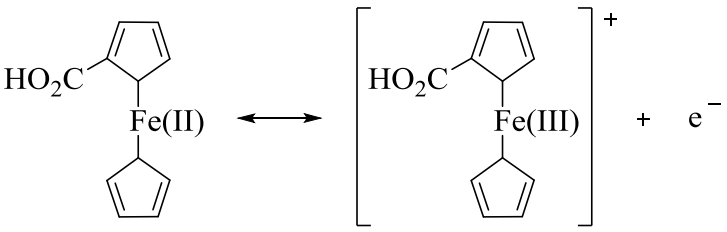

Equation 1.3

Recently, detection of the intrinsic oxidation of G and A nucleotides has been used as a label-free approach to determine hybridisation, with a change in oxidation signal observed following hybridisation.[27,50] Both of these purines are electroactive with a greater Faradaic charge being exhibited following DNA hybridisation.[57] Li *et al.*[50] reported a label-free biosensor which detected the intrinsic oxidation of purine bases, with an increase in purine base oxidation signal observed following the hybridisation event. Another approach to direct oxidation of adenine and guanine oxidation is through the modification of probe sequences with G bases substituted with inosine to reduce background current through the presence of fewer electroactive bases in probe sequences.[1] While label-free detection using the intrinsic oxidation properties of purine bases is simple and convenient, signal intensity is generally poorer than other detection techniques, due to a larger background current and therefore a decreased signal to noise ratio.[57] Additionally these biosensors cannot be easily regenerated following measurement as the oxidation event is an irreversible process, limiting the potential application of intrinsic purine oxidation as a feasible label-free detection strategy.[50]

1.3 Scope of present study

The primary aim of this work was to develop a label-free electrochemical DNA biosensor for the *in vitro* monitoring of DNA hybridisation using sequences related to BRCA1, as model biological analytes. A series of *BRCA1* DNA sequences, including those shown in Figure 1.3, were designed for *in vitro* experimentation to mimic loss of protein functionality caused by the introduction of a stop codon into the gene sequence of regions of the *BRCA1* gene. These sequences formed the basis of the biorecognition element on the developed DNA biosensor.

The structure of DNA biosensor, shown in Figure 1.4, was based on a nanomaterial modified glassy carbon electrode transducer surface, including graphene, an amine linker and gold nanoparticles incorporated through stable C-Au bonds. Unlike many approaches where individual parameters were optimised in an attempt to determine the greatest performance,[14,23,63,64] a two-level factorial experimental design was employed to identify the significant factors and interactions in the development of the biosensor platform. Finally, ssDNA probe sequence was bonded, through thiol-gold chemistry, to gold nanoparticles and Zr(IV) was coordinated in the hybridised dsDNA duplex, on the electrode surface. Zirconia was incorporated to attract an oxygen containing redox marker, ferrocenecarboxylic acid (Equation 1.3), to the biosensor surface for sensitive quantitative detection of *BRCA1* related gene sequences. Notably, a unique feature of this electrochemical DNA biosensor design lies in the combined nanomaterial approach employed and the diazonium-based technique for the incorporation of gold nanomaterials through C-Au bonds, rather than the less stable and commonly reported NH-Au bonding approach.[35,36]

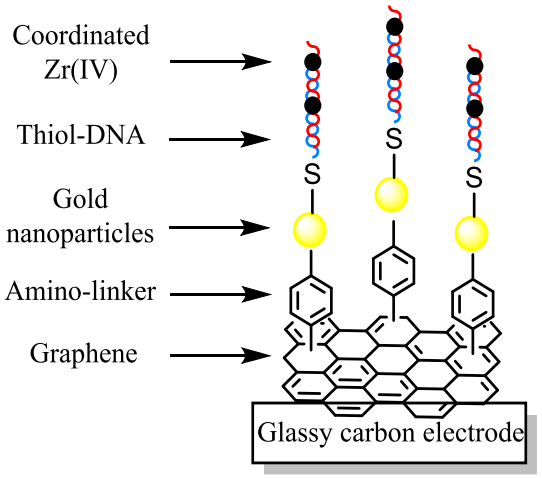

Figure 1.4 Overall design of the glassy carbon-based electrochemical DNA biosensor for the detection of *BRCA1* related gene sequences.

Characterisation of the developed biosensors was performed using voltammetric-based techniques including cyclic voltammetry and square wave voltammetry. Cyclic voltammetry was utilised to analyse the change in electrochemical response of an electrochemical redox marker following the modification of the electrochemical biosensor transducing element. The signals obtained by cyclic voltammetry were also used as the independent variable response values to perform full factorial designs. EIS was then used to determine the impedance of the biosensor platform following the addition of optimised surface layers on the transducing surface. Finally, square wave voltammetry was used in calibration experiments to quantitatively study the analytical performance of the biosensors for the monitoring of DNA hybridisation using *BRCA1* related DNA sequences as model biological analytes.

Chapter 2

EXPERIMENTAL

2.1 Introduction

The primary aim of this work was to develop a label-free electrochemical DNA biosensor for the *in vitro* monitoring of DNA hybridisation using *BRCA1* related gene sequences as model biological analytes. To achieve this aim, our label-free biosensor design was based on a biosensing platform consisting of electro-reduced graphene oxide, an aryl diazonium linker and gold nanoparticles, on a glassy carbon electrode. To this anchoring layer, a 19 mer oligonucleotide thiol-labelled DNA probe was attached using thiol-gold covalent bonding, followed by hybridisation with its complementary target, a *BRCA1* related DNA sequence. Finally, Zr(IV) was coordinated into the DNA duplex. In our work, a two-level factorial design approach was used for experimental factor optimisation and identification of the significant factors and their interactions in biosensor performance. Characterisation and analytical performance of the developed biosensor was performed by cyclic voltammetry, square wave voltammetry and EIS. The present chapter outlines the detailed descriptions of the instrumentation and experimental procedures adopted such that the most reliable results were obtained. Results obtained in this manner are presented and discussed in Chapter 3.

2.2 Reagents

Absolute ethanol, graphite powder (1-2 μm), potassium persulfate, phosphorous pentoxide, sodium nitrate, potassium permanganate, sodium chloride, potassium chloride, potassium nitrate, hydrogen peroxide (30% wt/v), sodium hydroxide, *p*-phenylenediamine, sodium nitrite, gold(III) chloride trihydrate, hexaammineruthenium(III) chloride, ferrocenecarboxylic acid and RNase and DNase free tris-ethylenediaminetetraacetic acid (EDTA; TE) buffer (1.0 M Tris-HCl, 0.1 M EDTA) were all purchased from Sigma Aldrich (Australia) and were used without any further purification. Disodium hydrogen phosphate, potassium dihydrogen orthophosphate, hydrochloric acid (37% v/v) and sulfuric acid (98% v/v) were purchased from Ajax Finechem Pty Ltd (Australia). Potassium ferrocyanide, tri-sodium citrate and zirconyl chloride octahydrate were purchased from British Drug House Ltd (USA). Potassium ferricyanide was purchased from May and Baker Ltd (England). Alumina powder

(0.05, 0.3 and 1 μm) was purchased from Leco Corporation Pty Ltd (Australia). Anhydrous *N,N*-dimethylformamide (DMF) was purchased from Merck Millipore (Australia). Tris-(2-carboxyethyl)phosphine hydrochloride (TCEP), ultrapure DNASE and RNASE-free water and DNA oligonucleotides were purchased from Invitrogen Australia Pty Ltd (Australia). Nitrogen used was high purity grade gas (BOC, Australia).

Synthetic 19 mer oligonucleotides relating to *BRCA1* gene sequences were commercially prepared with desalting purification and received lyophilised from Invitrogen Australia Pty Ltd (Australia). Oligonucleotides sequences, 5'- to 3, of thiol-modified DNA probe (molecular weight 6045 g mol^{-1}), target (molecular weight 5897 g mol^{-1}), three-base mismatched (molecular weight 5823 g mol^{-1}), single-base mismatched (molecular weight 5872 g mol^{-1}), and non-complementary (molecular weight 5730 g mol^{-1}) sequences are shown below.

Thiol-modified DNA probe:	HS-$(CH_2)_6$-GAT TTT CTT CCT TTT GTT C
Target DNA:	GAA CAA AAG GAA GAA AAT C
Three-base mismatched DNA:	GAA CAA ATC TAA GAA AAT C
Single-base mismatched DNA:	GAA CAA AAG GAA TAA AAT C
Non-complementary DNA:	ACT TGC TTA TCC TCT GTA A

DNA oligonucleotides were reconstituted with TE buffer (10 mM Tris-HCl, 1 mM EDTA) and 300 μM ssDNA stock solutions were prepared. Target ssDNA oligonucleotide solutions were prepared by dilution of 300 μM stock solutions to produce 3 μM working stock solutions and then dilution with TE buffer to obtain DNA oligonucleotides of appropriate concentrations. Oligonucleotides solutions were stored at 4 ºC and thermally denatured by heating at 90 ºC for 5 min immediately prior to use. All pipette tips and tubes used for DNA preparation were sterilised by autoclaving for 20 min (120 ºC). All DNA solution preparation was performed using aseptic techniques and solutions used for DNA preparation were RNase and DNase free and used as received.

Phosphate-buffered saline (PBS, pH 7.4), was prepared with 10 mM disodium hydrogen phosphate, 1.8 mM potassium dihydrogen orthophosphate, 137 mM sodium chloride and 2.7 mM potassium chloride. All solutions were prepared using deionised water (Direct-Q Millipore system) unless otherwise specified. In all experiments, pH values were measured

using an Orion 3 Star pH Meter (Thermo Scientific, USA) and 8157BNUMD Ross Ultra pH/ATC Triode pH probe (Thermo Scientific, USA), calibrated using a three point calibration using Orion pH Buffer (pH 4.01, 7.00 and 10.01, Thermo Scientific, USA,) prior to use, and pH was adjusted using HCl or NaOH.

2.3 Electrochemical instrumentation

All electrochemical measurements were performed using a three-electrode system consisting of a 3 mm diameter glassy carbon working electrode, a Ag|AgCl reference electrode (3 M KCl; both from Bioanalytical Systems Inc., USA) and a platinum/ titanium wire auxiliary electrode (eDAQ Pty Ltd, Australia). These electrodes were accommodated in a 40 mL cell with a fitted plastic lid for the three electrodes and a nitrogen gas inlet. Solutions were purged with water saturated nitrogen gas for 5 min prior to each series of experiments and solutions were covered with a blanket of nitrogen during analysis. All electrochemical potentials were obtained in a steel Faraday cage and are reported at room temperature against the Ag|AgCl reference electrode.

Voltammetric experiments were performed using an EA164 QuadStat potentiostat and an E-corder 410 data acquisition system (eDAQ Pty Ltd, Australia), interfaced with a desktop computer (Windows XP) via EChem v2.1.13 software (eDAQ Pty Ltd, Australia). Cyclic voltammetry (scan rate = 100 mV s^{-1}) and square wave voltammetry (scan rate = 100 mV s^{-1}, frequency = 25 Hz, pulse height = 2 mV, amplitude = 25 mV) was performed to characterise the electrode response to several redox markers including 4 mM of the positively charged $Ru(NH_3)_6^{3+/2+}$ in PBS at pH 3 and pH 6, 1 mM each of the negatively charged $Fe(CN)_6^{3-}$ / $Fe(CN)_6^{4-}$ in 0.1 M KNO_3 redox couple and 1 mM of the neutral ferrocenecarboxylic acid in pH 7.4 PBS.

EIS was performed using an Autolab PGStat12 (MEP Instruments Pty Ltd, Australia), interfaced with a desktop computer (Windows 7) via Frequency Response Analysis (FRA) v4.9.007 software (MEP Instruments Pty Ltd, Australia). EIS measurements of the optimised electrochemical DNA biosensor platform was performed using 1 mM $Fe(CN)_6^{3-}$ / 1 mM $Fe(CN)_6^{4-}$ in 0.1 M KNO_3 supporting electrolyte as the redox marker. An alternating potential of 10 mV in amplitude in the frequency range of 10 kHz to 0.1 Hz, spaced logarithmically, was superimposed on the applied DC potential, which corresponded to the half-wave potential independently determined by cyclic voltammetry for each electrode. Nyquist plots were

prepared and Frequency Response Analysis v4.9.007 software was used to fit results to the Randles circuit model until good agreements were obtained.

2.4 Electrode preparation

All glassy carbon electrodes were rinsed and then ultrasonicated in ethanol for 5 min, followed by deionised water for a further 5 min in a Cole-Parmer CP130 Ultrasonic Processor ultrasonicator (Extech Equipment Pty Ltd, Australia). The electrodes were subsequently polished to a mirror finish using slurries of 1.0, 0.3 and 0.05 μm alumina powder on microcloth polishing pads (Leco Australia Pty Ltd, Australia) for 3 min. Between polishing stages, the electrodes were rinsed and ultrasonicated in deionised water for 3 min before finally being ultrasonicated with deionised water for a further 5 min and then dried with nitrogen gas prior to use.

2.5 Fabrication of glassy carbon electrode sensing platform

2.5.1 Preparation of graphite oxide

Graphite oxide was prepared according to a modified Hummers method.[30,35,41] Briefly, potassium persulfate (2.5 g) and phosphorous pentoxide (2.5 g) were dissolved in sulfuric acid (12 mL). The mixture was stirred until dissolved and then heated to 80 °C prior to the addition of graphite powder (1.5 g). The solution was stirred at 80 °C for 5 h, before being cooled to room temperature. The solution was diluted with deionised water (500 mL) and vacuum filtered with 5.5 cm Grade 1 Qualitative Filtration Paper (Whatman, USA) to obtain black, pre-oxidised graphite, which was rinsed with deionised water and dried overnight in a vacuum desiccator.

Pre-oxidised graphite (1 g) and sodium nitrate (1 g) were then dissolved in sulfuric acid (46 mL). The solution was stirred at 0 °C for 10 min. Potassium permanganate (6 g) was then slowly added over a 1 h period with continual stirring, after which the mixture was heated to 35 °C for 1 h. The mixture was next diluted with deionised water (80 mL) and heated to 90 °C for 30 min. The oxidation process was terminated by the addition of water (200 mL) and 30% (wt/v) hydrogen peroxide (6 mL). The dark orange/ light brown solution was then was vacuum filtered with 5.5 cm Grade 1 Qualitative Filtration Paper (Whatman, USA), washed three times with 5% HCl (200 mL) and finally three times with deionised water (200 mL). A light brown solid material was obtained and dried in a vacuum desiccator to afford graphite oxide.

2.5.2 Preparation of graphene oxide

Due to the long-term stability of graphite oxide in DMF and the feasibility to produce single-layer graphene oxide by ultrasonication,[65] anhydrous DMF dispersions of 2.0 mg mL^{-1} graphite oxide were ultrasonicated before being applied to a glassy carbon electrode.

2.5.3 Immobilisation of graphene on glassy carbon electrodes

Graphene oxide was immobilised by applying graphene oxide suspensions (5 μL of 2.0 mg mL^{-1}) on a dry, polished glassy carbon electrode, before this was dried in a vacuum desiccator. Electrochemical reduction of graphene oxide modified electrodes was then performed by applying a potential of -1.3 V for 5 min to produce electrochemically reduced graphene oxide (ERGO)-modified glassy carbon electrode (ERGO-glassy carbon electrode). The reduction potential applied was selected from cyclic voltammetric analysis of graphene oxide modified electrodes in pH 7.4 PBS (see Figure 3.2 in Chapter 3).

2.5.4 ERGO-glassy carbon electrode surface modification with *in situ* generated aryl diazonium cations

Amine groups were incorporated on ERGO-glassy carbon electrodes after electrochemically reducing *in situ* generated aryl diazonium cations on the electrodes in acidic solutions, as described previously.[35,36] Briefly, 1 mM sodium nitrite (final concentration) was added to a 0.5 M aqueous HCl solution of 1 mM *p*-phenylenediamine. The mixture was degassed and stirred in an ice bath while being kept in darkness for 15 min. Electrochemical reduction of *in situ* generated, *p*-phenylenediamine diazonium salts was then conducted at the electrode by scanning the potential between 0.6 V to -1.0 V for two cycles at a scan rate of 100 mV s^{-1} to generate NH_2-ERGO-glassy carbon electrode. The electrodes were washed well and air dried in a desiccator until required.

2.5.5 Gold nanoparticle modified electrode

The biosensing platform was completed by incorporating gold nanoparticles (AuNPs) to obtain AuNP-4-phenyl(Ph)-ERGO-glassy carbon electrodes using diazonium chemistry.[36] Gold nanoparticles were prepared by the addition of 200 μL 40 mM trisodium citrate solution to a boiling solution of 1 mM $HAuCl_4$, under reflux, in deionised water with constant stirring. A colour change from light yellow to dark red was observed after approximately 30 s, which was consistent with reports of gold nanoparticle formation using sodium citrate.[36,66] NH_2-ERGO-glassy carbon electrodes were incubated in a 0.5 M aqueous HCl solution of

5 mM sodium nitrite for 15 min to generate $N_2^+Cl^-$-Ph-ERGO-glassy carbon electrodes. Gold nanoparticles were then covalently attached to the biosensing surface by performing cyclic voltammetry of the $N_2^+Cl^-$-Ph-ERGO-glassy carbon working electrode in the gold nanoparticle solution, cycling between 0.6 V and -0.8 V for two cycles at a scan rate of 100 mV s^{-1} to obtain AuNP-Ph-ERGO-glassy carbon electrodes. The electrodes were washed well and air dried in a desiccator until required.

2.6 Detection of DNA hybridisation

The performance of the electrochemical DNA biosensor was analysed using an adapted procedure by Wipawakarn *et al.*[13] for the monitoring of DNA hybridisation and *BRCA1* related gene sequences were used as model analytes. Initially any disulfide bonds, which may be present in the thiol-labelled probe ssDNA solution, were reduced using TCEP. A 3 µL aliquot of 300 µM ssDNA probe was combined with 12 µL of 10 mM TCEP and left to incubate in the dark for 30 min at 4 ºC. Then, 75 µL TE buffer was added to dilute the ssDNA solution to a concentration of 10 µM and the diluted ssDNA solution was thermally denatured. Finally ssDNA was immobilised on the AuNP-Ph-ERGO-glassy carbon electrodes by applying a 5 µL aliquot of the reduced, denatured 10 µM ssDNA probe, which was left to air dry in a desiccator for 1 h. The ssDNA modified electrode was rinsed in TE buffer for 15 s to remove any unbound ssDNA oligonucleotides and then incubated in a 10 mM Zr(IV) containing solution for 15 min. The ssDNA electrode was rinsed with PBS for 15 s to remove any unbound Zr(IV) before being characterised using cyclic voltammetry and square wave voltammetry of 1 mM $Fe(CN)_6^{3-}$ / 1 mM $Fe(CN)_6^{4-}$ in 0.1 M KNO_3 and 1 mM ferrocenecarboxylic acid in pH 7.4 PBS and then rinsed with water.

Hybridisation of ssDNA target oligonucleotides with target sequences was then performed. Target oligonucleotides were thermally denatured and then incubated at 37 ºC before the ssDNA probe modified electrodes were allowed to hybridise with complementary DNA of specific concentrations (10-100 nM) at 37 ºC for 15 min. The electrodes were then rinsed with TE buffer, incubated in 10 mM Zr(IV) for 15 min, washed with PBS and then characterised with cyclic voltammetry and square wave voltammetry of 1 mM $Fe(CN)_6^{3-}$ / 1 mM $Fe(CN)_6^{4-}$ in 0.1 M KNO_3 and 1 mM ferrocenecarboxylic acid in pH 7.4 PBS.

2.7 Characterisation of graphite oxide

Fourier transform infrared (FTIR) spectroscopy was used to characterise synthesised graphite oxide. FTIR was performed using a Nicolet IS5 FTIR spectrometer equipped with an iD5 attenuated total reflectance (ATR) diamond plate and data analysis performed using OMNIC software v8.2 (Thermo Scientific, USA). FTIR spectra were collected from 650-4000 cm^{-1} at a resolution of 4 with spectra obtained from an average of 16 scans.

2.8 Statistical analysis

All errors presented in this work are representative of the 95% confidence intervals for the mean values. A full two-level factorial design was used to identify significant factors, and their possible interactions, in optimising the composition of the AuNP-Ph-ERGO-glassy carbon electrode biosensing platform. The statistical significance of correlation coefficients was determined based on a two-tailed Student's *t* test.

Chapter 3

RESULTS AND DISCUSSION

3.1 Introduction

A long-term goal in the research area of electrochemical DNA biosensors is to be able to detect DNA hybridisation using miniature, portable, simple and cost effective devices. Electrochemical DNA biosensors offer great promise to point-of-care diagnostics, identification of mutations at the genomic level and personalised medicine. The general structure of an electrochemical DNA biosensor involves an electrochemical transducing element and a DNA biological recognition element. As reviewed in Chapter 1, a range of approaches to biosensor platform fabrication and biological element immobilisation have been reported in literature, with the transducing element generally affecting sensitivity and the biological recognition element imparting selective detection. For the detection of nucleic acids, a ssDNA oligonucleotide is immobilised on an electrode surface, and upon exposure to a complementary DNA sequence, hybridisation occurs. One way in which hybridisation can be detected is simply based on the electroactivity of redox markers in label-free approaches. A number of analytical performance parameters including good sensitivity, selectivity enabling the detection of single mismatched DNA sequences, limit of detection, dynamic range and reproducibility characteristics will determine the effectiveness of an electrochemical DNA biosensor.

In this work, the above parameters of electrochemical detection and effective DNA biosensors were considered to develop a label-free electrochemical DNA biosensor for *in vitro* DNA hybridisation detection using the model, biologically important analytes, *BRCA1* related gene sequences. Our label-free biosensor (shown in Figure 1.4) consisted of a factorial design optimised, nanomaterial-based transducer surface, with electro-reduced graphene oxide, an aryl diazonium linker and gold nanoparticles modified glassy carbon electrodes. The biological recognition element was based on *BRCA1* related gene sequences and incorporated zirconium following the hybridisation event, for enhanced sensitivity to detection of oxygen-containing redox markers.

3.2 Preparation of bare glassy carbon electrodes

In this work, glassy carbon electrodes were selected as the transducing element due to the useful mechanical and electrical properties, wide potential window, ability for surface modification and the relatively reproducible performance of glassy carbon electrodes.[67] When developing an electrochemical DNA biosensor with a modified transducer surface, in this case glassy carbon electrodes, it is imperative to prepare the surface prior to modification. To ensure that the glassy carbon electrode surface was uniform and contaminant-free prior to use, a cleaning process was performed immediately prior to use, involving mechanical polishing with alumina powder and ultrasonication in ethanol and deionised water. Cyclic voltammetry of 1 mM ferrocenecarboxylic acid in pH 7.4 PBS was conducted at this electrode with the overlaid cyclic voltammograms and peak current versus (potential scan rate)$^{1/2}$ plot shown in Figures 6.1 (a) and (b) in Supplementary Material. Based on a peak separation of 73 ± 11 mV, a current peak ratio of 0.99 ± 0.02 (where the errors represent 95% confidence intervals) and a linear peak current versus (potential scan rate)$^{1/2}$ plot (statistically significant correlation coefficient of 0.9999 and -0.9999 for the cathodic plot and anodic plot, respectively (N=8), at 95% confidence level), the expected quasi-reversibility was observed for the redox reaction of ferrocenecarboxylic acid at the glassy carbon electrode.[68,69]

3.3 Fabrication of biosensing platform

3.3.1 Immobilisation of graphene on glassy carbon electrodes

Following the preparation and characterisation of bare glassy carbon electrodes, the biosensing platform was initially assembled by immobilising electrochemically reduced graphene oxide. Graphene was used in this work to exploit its excellent electrical conductivity of the material, fast electron transfer and the large surface area.[30,32,39,40] Graphene was immobilised on the biosensing platform by electrochemically reducing graphene oxide on the glassy carbon electrode. Initially, graphite oxide was prepared from graphite according to a modified Hummers method.[30,35,41] To confirm the successful synthesis of graphite oxide, ATR spectroscopy was employed to obtain an FTIR spectrum of graphite oxide and the starting material graphite. Spectra were collected from an average of 16 scans and the spectra of graphite oxide and graphite are depicted in Figure 3.1. The FTIR spectrum of graphite oxide exhibits peaks at 3700–2600 cm^{-1}, 1800-1700 cm^{-1} and 1700-1650 cm^{-1}. These peaks were attributed to O-H stretching, carboxyl C=O and ketonic C=O stretching vibrations, respectively, and are consistent with those previously reported for graphite oxide synthesised through a modified Hummers method.[70] As the spectrum of the

starting material, graphite, only exhibits alkene-based peaks at 2000 cm^{-1}, FTIR analysis of graphite oxide confirms successful oxidation of graphite by the method employed.

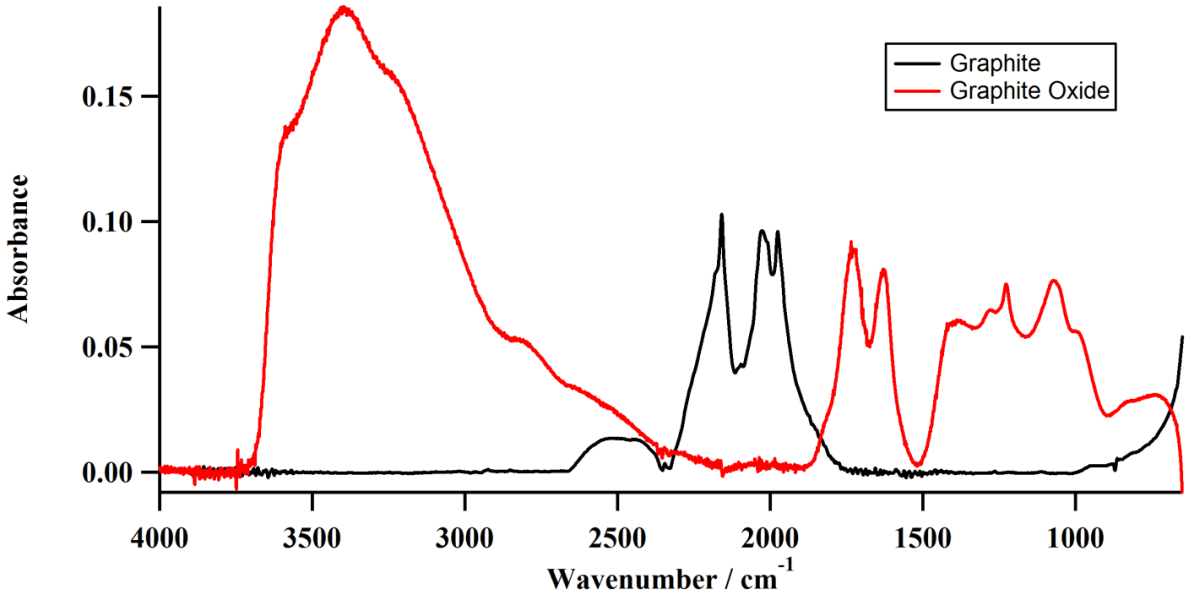

Figure 3.1 Overlaid infrared spectra of graphite and graphite oxide. Spectra collected from ATR with a diamond plate and baseline correction applied.

The graphene oxide was next immobilised on glassy carbon electrodes prior to electrochemical reduction. Graphite oxide in DMF (2 mg mL^{-1}) was ultrasonicated to cleave hydrogen bonds between graphene oxide sheets and produce single layer graphene oxide sheets.[32,39,65] DMF was used as the solvent to prepared graphite oxide solutions due to the long-term stability of graphite oxide in DMF.[39,65] After placing an aliquot of graphene oxide suspension on a polished glassy carbon electrode and dried in a vacuum desiccator, graphene oxide was secured on the electrode surface by π- π stacking.[30] This then produced a graphene oxide-glassy carbon electrode.

Finally, graphene oxide-glassy carbon electrodes were reduced to produce graphene modified glassy carbon electrodes. As "green chemistry" approaches are favourable in the development of biosensors, electrochemical reduction of graphene oxide was performed, rather than the use of hazardous and environmentally damaging chemical reducing agents and to avoid potential contamination of the reduced product.[71] To determine the appropriate reduction potential to electrochemically reduce graphene oxide-glassy carbon electrodes from graphene oxide modified electrodes, cyclic voltammetry of a graphene oxide-modified electrode in PBS was performed and the voltammograms obtained are shown in Figure 3.2.

The potential was ramped from 0.0 to -1.5 V and the current exhibited a large, irreversible cathodic peak at -1.3 V which decreased over subsequent scans. This cathodic peak current was attributed to the reduction of surface oxygen groups of graphene oxide as the reduction of water occurs at more negative potentials.[71] ERGO-glassy carbon electrodes were produced by the application of a reduction potential of -1.3 V for 5 min and the amperometric signal obtained is shown in Figure 3.3. This result shows that reduction commencing immediately after the application of the reduction potential. A constant current was observed after 150 s, indicating that the reduction event was completed over the period of the reduction scan.

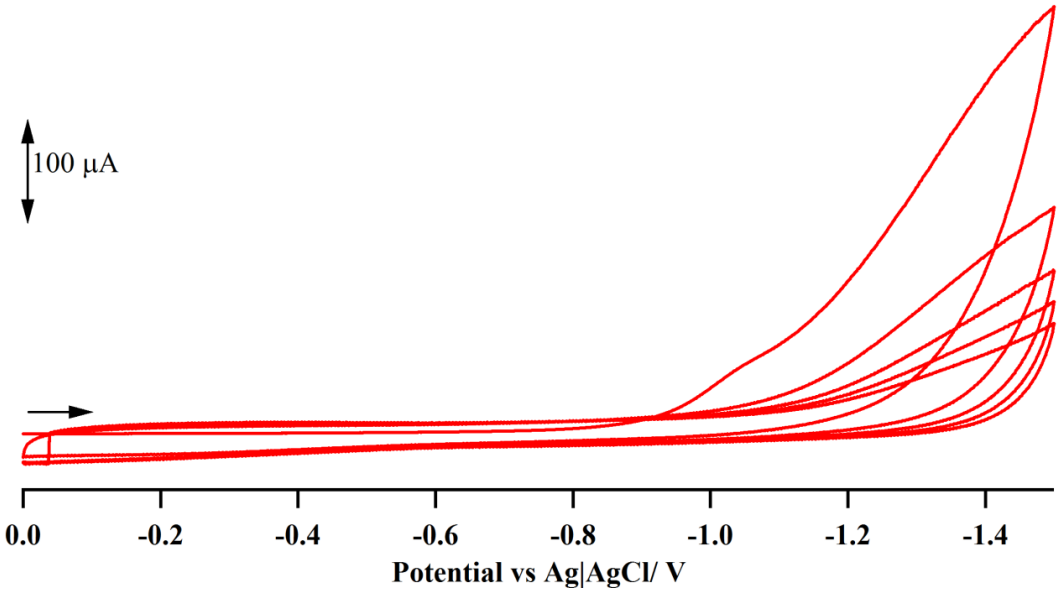

Figure 3.2 Subsequent cyclic voltammogram scans of a graphene oxide-glassy carbon electrode in pH 7.4 PBS; scan rate = 100 mV s^{-1}. The arrow shows the initial scan direction.

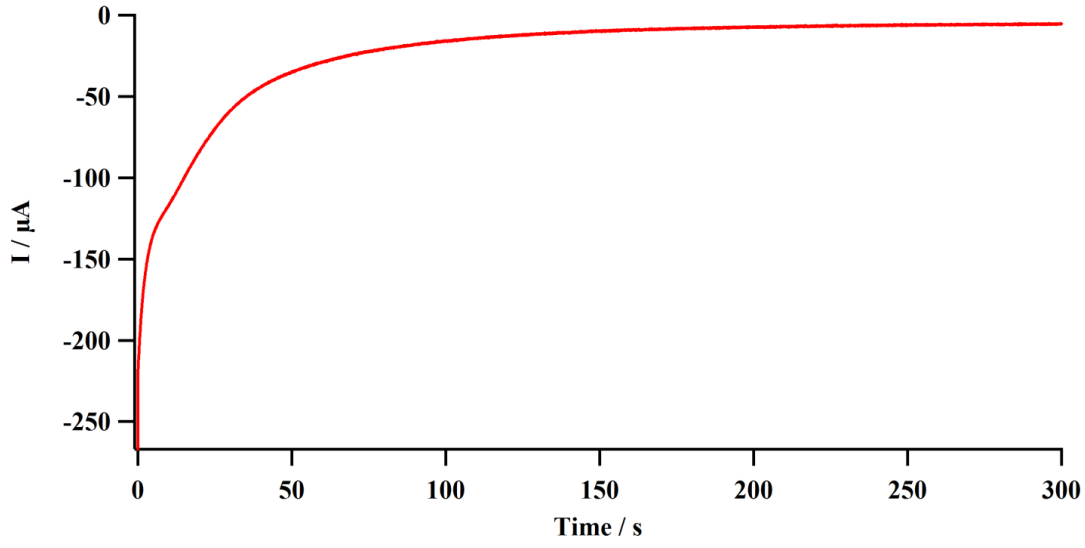

Figure 3.3 Reduction of a graphene oxide-glassy carbon electrode in pH 7.4 PBS, by the application of a reduction potential of -1.3 V (determined by cyclic voltammetry); scan rate = 100 mV s^{-1}.

3.3.2 ERGO-glassy carbon surface modification with *in situ* generated aryl diazonium cations

Aryl diazmonium chemistry has been reported to produce organic layers with signicantly increased stability compared to alkanethiol self-assembled monolayers on gold electrodes.[36] Accordingly, our biosensing platform incorporated an amine linking layer that offered sites for the covalent attachment of gold nanoparticles, minimising agglomeration, to subseqently attach the thiol-labelled ssDNA recognition element. The *in situ* formation of aryl diazonium cations was performed by the reported reaction of sodium nitrite, HCl and an aryl amine,[35,36,49] prior to the electrochemical reduction of the diazonium salt by cyclic voltammetry. This reaction facilitates the formation of irreversible, strong C-C bond formation (bond strength 100 kcal mol^{-1}).[72] This approach to diazonium cation surface modification is schematically shown in Figure 3.4, with formation of the diazonium cation followed by electrochemical reduction to form strong C-C bonds. In this scheme, two amine groups of *p*-phenylenediamine, both of which could potentially undergo formation of a bifunctional diazonium salt and facilitate uncontrolled attachment of the aryl amine to the electrode surface, are present. However it has been reported that upon exposure of *p*-phenylenediamine to sodium nitrite, only one of the amine groups is converted to the diazonium cation.[73] Chen *et al.*[74] hypothesised that the absence of the second diazonium moiety is attributed to the result of a more spontaneous one-electron only reduction at the electrode surface.

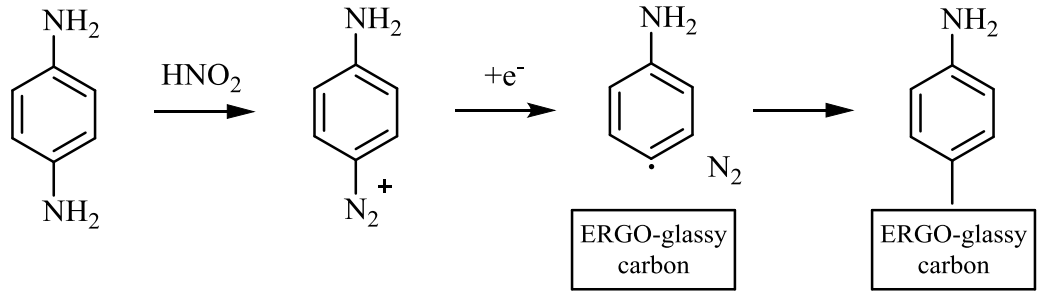

Figure 3.4 Simplified diazonium reaction mechanism of grafting amine groups on the surface of ERGO-glassy carbon electrodes. The reaction involved sodium nitrite, HCl and *p*-phenylenediamine reacting to generate NH_2-ERGO-glassy carbon electrode.

Next, *in* situ generated diazonium cations were reduced by two cyclic voltammetric scans between 0.6 and -1.0 V to generate aryl radicals that react rapidly with the electrode surface to form irreversible C-C bonds. The cyclic voltammograms obtained are shown in Figure 3.5. Two reduction peaks, at 0.42 V and -0.10 V, were identified in the cyclic voltammograms.

The quasi-reversible peak at 0.42 V was attributed to the reduction of the diazonium salt, producing the aryl radical and release of nitrogen, and the irreversible peak at -0.10 V was attributed to the formation of a covalent C-C bond to the electrode surface.[35,49] The second scan showed suppression of the reduction peak at -0.10 V, suggesting surface saturation and the successful covalent attachment of aryl amine groups on the electrode surface.

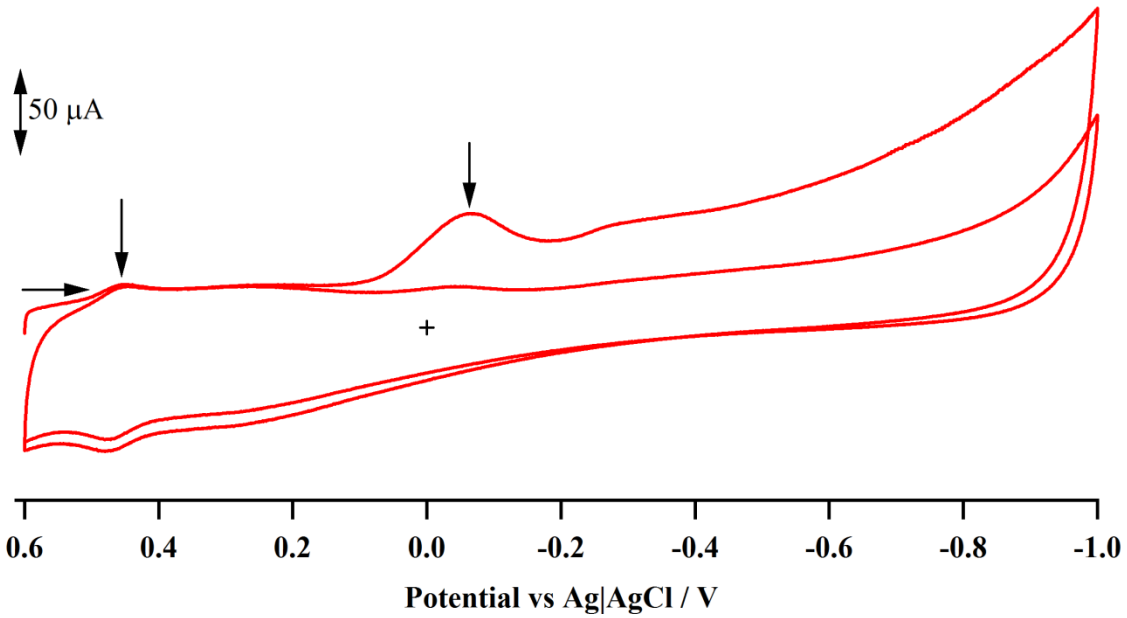

Figure 3.5 Cyclic voltammograms obtained over two scans of an ERGO-glassy carbon electrode in diazonium generating solution (1 mM sodium nitrite, 0.5 M aqueous HCl and 1 mM *p*-phenylenediamine) at a scan rate of 100 mV s^{-1}. The arrow shows the initial scan direction and the cross indicates the origin.

A separate experiment was performed to confirm the presence of an amine layer on the electrode surface before adding gold nanoparticles to complete the electrochemical biosensing platform. Tasca *et al.*[73] reported the pK_a of *p*-phenylenediamine on carbon nanotube modified glassy carbon electrodes as 4.6. This property of the amine layer can therefore be exploited by monitoring the electrochemical response of a charged redox marker at selected pH values to confirm the presence of the grafted layer on the electrode surface. Cyclic voltammetry of the positively charged $Ru(NH_3)_6^{3+/2+}$ redox couple at pH values above and below the pK_a of the amine group, was performed to characterise the NH_2-ERGO-glassy carbon electrodes. More specifically, cyclic voltammetry, from 0.1 to -0.6 V, of 4 mM $Ru(NH_3)_6^{3+}$ in pH 3 and pH 6 PBS at NH_2-ERGO-glassy carbon electrodes was performed and the results obtained are presented in Figure 3.6. At pH 3, most amine groups are protonated and positively charged, and at pH 6, the surface groups are neutral. This is confirmed in the cyclic voltammograms in Figure 3.6 with signal suppression in the scan performed at pH 3, likely due to the electrostatic repulsion of the positively charged redox marker, and an unaffected signal when

analysed at pH 6, due to no electrostatic repulsion. These results strongly suggest the successful grafting of the *p*-phenylenediamine amine layer to produce NH_2-ERGO-glassy carbon electrodes.

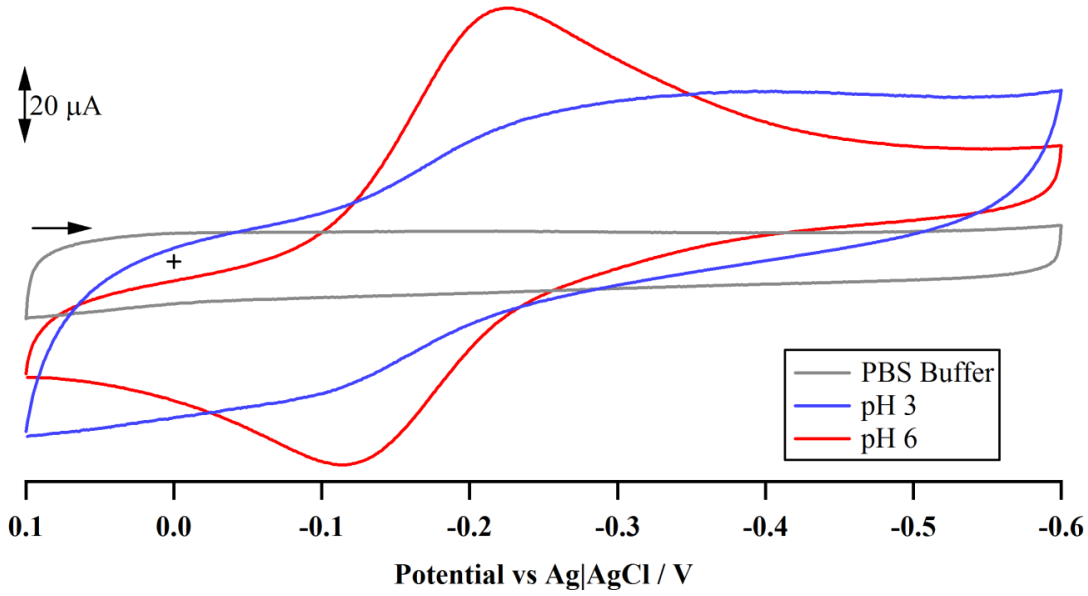

Figure 3.6 Cyclic voltammograms of 4 mM hexaaminеruthenium(III) chloride in PBS, analysed using NH_2-ERGO-glassy carbon electrodes at a scan rate of 100 mV s^{-1}. The analysis was performed at two different pH values, pH 3 and 6, and also in the absence of hexaaminеruthenium(III) chloride as a control. The arrow shows the initial scan direction and the cross indicates the origin. The third scan of each pH condition is shown in this figure.

3.3.3 Gold nanoparticle modified electrode surface

The final step of assembling the biosensing platform design involved the addition of gold nanoparticles to the NH_2-ERGO-glassy carbon modified electrodes. Gold nanoparticles have been incorporated in biosensor designs to increase the sensitivity of biosensor and as a means to impart selectivity though subsequent attachment of the biosensing element.[36] In our biosensor design, gold nanoparticles were incorporated to utilise these advantageous properties of gold nanoparticles and as the anchoring platform for ssDNA to be covalently attached. As discussed in Chapter 1, gold nanoparticles can be synthesised through a variety of synthetic approaches including both chemical[35,46] and electrochemical reduction[35,47] of chloroauric acid. Gold-carbide bonds (bond strength of 317 kJ mol^{-1}) were reported as having superior stability to NH-Au bonds (bond strength of 154 kJ mol^{-1}),[36] and as a result, a chemical reduction and an electrochemical diazonium reduction method was selected as the synthetic approach to incorporating gold nanoparticles in the biosensor design through C-Au covalent bonding.

To synthesise gold nanoparticles, chloroauric acid was initially chemically reduced to form citrate-capped gold nanoparticles.[36,66] In this approach reported by Frens,[66] the quantity of sodium citrate added was experimentally determined to affect the size of the gold nanoparticles synthesised. This approach facilitated a convenient method for synthesising different sized gold nanoparticles, with the relationship between quantity of reducing agent and diameter of nanoparticles reported.[66] After approximately 30 s following the addition of 200 μL of 0.04 M sodium citrate solution, a dark red suspension of gold nanoparticles was obtained. In a previous work,[66] an average diameter of 16 nm was estimated for gold nanoparticles synthesised in a similar manner. A second diazonium reaction, analogous to that outlined in Figure 3.4, was performed utilising the free aryl amine on the modified electrode surface. The NH_2-ERGO-glassy carbon electrodes were incubated in an aqueous HCl solution of sodium nitrite, to generate $N_2^+Cl^-$-Ph-ERGO-glassy carbon electrodes, followed by electrochemical reduction in the gold nanoparticle solution, shown in Figure 3.7. The figure shows the Faradaic reduction of a diazonium cation to produce a phenyl radical, consistent with similar diazonium reactions in nanoparticle solutions.[36] In the presence of gold nanoparticles, the formation of a C-Au bond facilitated the immobilisation of gold nanoparticles that were strongly covalent-bonded to produce the AuNP-Ph-ERGO-glassy carbon electrodes. These gold nanoparticles then formed the basis for immobilisation of a ssDNA probe.

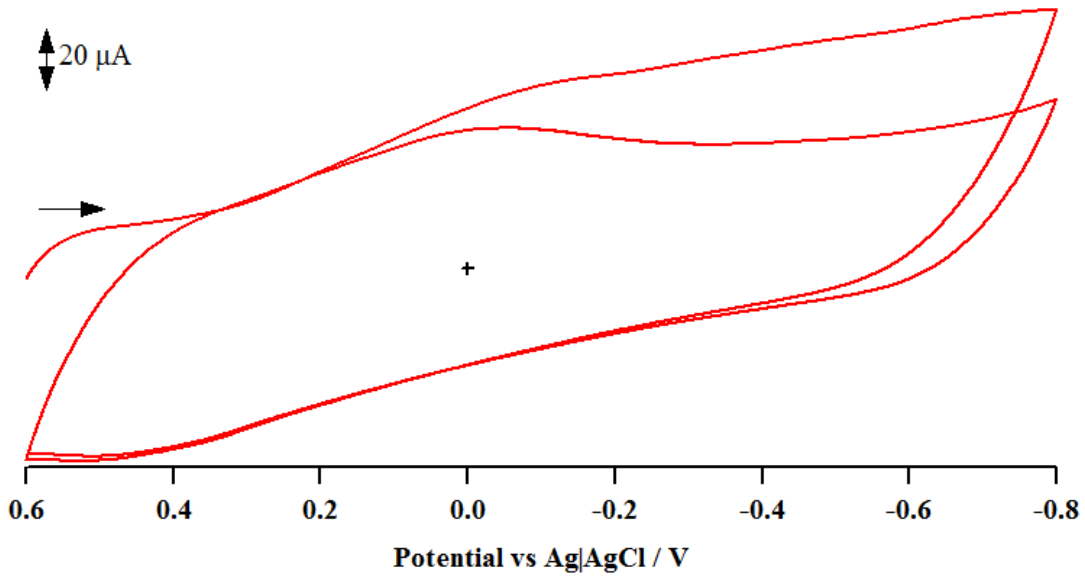

Figure 3.7 Cyclic voltammograms obtained over two scans of a $N_2^+Cl^-$-Ph-ERGO-glassy carbon electrode in the presence of gold nanoparticle solution at a scan rate of 100 mV s^{-1}. The arrow shows the initial scan direction and the cross indicates the origin.

3.3.4 Factorial design optimisation

Immobilisation of a ssDNA probe on a modified biosensor platform directly affects the biosensor sensitivity, stability, surface functionality, probe density and accessibility for DNA hybridisation.[59] Therefore the composition of the biosensor platform is an important consideration in development of electrochemical DNA biosensors. Many approaches involving study of parameters being individually optimised to achieve the highest biosensor platform performance,[14,23,63,64] with such approaches being inefficient and unable to identify any possible significant interactions between factors.[59] Instead, factorial designs offer a statistical-based technique to optimise biosensor platforms, with simultaneous evaluation of the effects of main factors and their interactions on the response signal.[13,59]

In this work, the ssDNA probe was immobilised on a nanomaterial-based biosensing platform consisting of electro-reduced graphene oxide, an aryl diazonium linker and gold nanoparticles modified glassy carbon electrodes. Three factors, concentration of graphene oxide immobilised on the electrode surface (denoted as X_1), concentration of *p*-phenylenediamine used in the diazonium reaction (X_2) and the volume of sodium citrate added for gold nanoparticles synthesis (X_3), were identified as factors contributing to the optimisation of the probe immobilisation platform. Accordingly, a full two-level 2^3 factorial design was used to identify significant factors and their possible interactions in optimisation of this biosensing platform, prior to attachment of the biorecognition element. These experimental factors, and their respective high and low levels, are shown in Table 3.1. Preliminary experimentation was performed to identify suitable ranges for the high and low factor values in Table 3.1. In determining the high and low concentrations of graphene oxide, a range between 0.1 mg mL^{-1} to 0.7 mg mL^{-1} of graphene oxide was immobilised on a glassy carbon electrode and cyclic voltammetric responses of 1 mM ferrocenecarboxylic acid in pH 7.4 PBS were conducted. Figure 3.8 (a) shows the cyclic voltammograms obtained. A linear oxidation peak current (at 0.33 V) versus graphene oxide concentration plot, shown in Figure 3.8 (b), indicated a low graphene oxide concentration of 0.2 mg mL^{-1}, while the high value of 2.0 mg mL^{-1} was selected based on limited solubility of graphene oxide suspensions in DMF above this concentration. A similar approach was performed to determine high and low levels for factor X_2 (5.0 and 0.5 mM, respectively), with an overlaid plot of cyclic voltammogram responses of 1 mM ferrocenecarboxylic acid in pH 7.4 PBS (Figure 3.9). Finally, the high and low levels for factor X_3 were determined as the volume of sodium citrate solution added directly affects the size and surface area of gold nanoparticles synthesised,[66] and the surface area of the

electrode will impact the amount of ssDNA which can be immobilised on the biosensor. Based on results reported by Frens,[66] the size of gold nanoparticles produced by addition of the low level of sodium citrate (60 µL) will be 72 nm and addition of the high level of sodium citrate (200 µL) will produce smaller nanoparticles with a diameter of 16 nm.

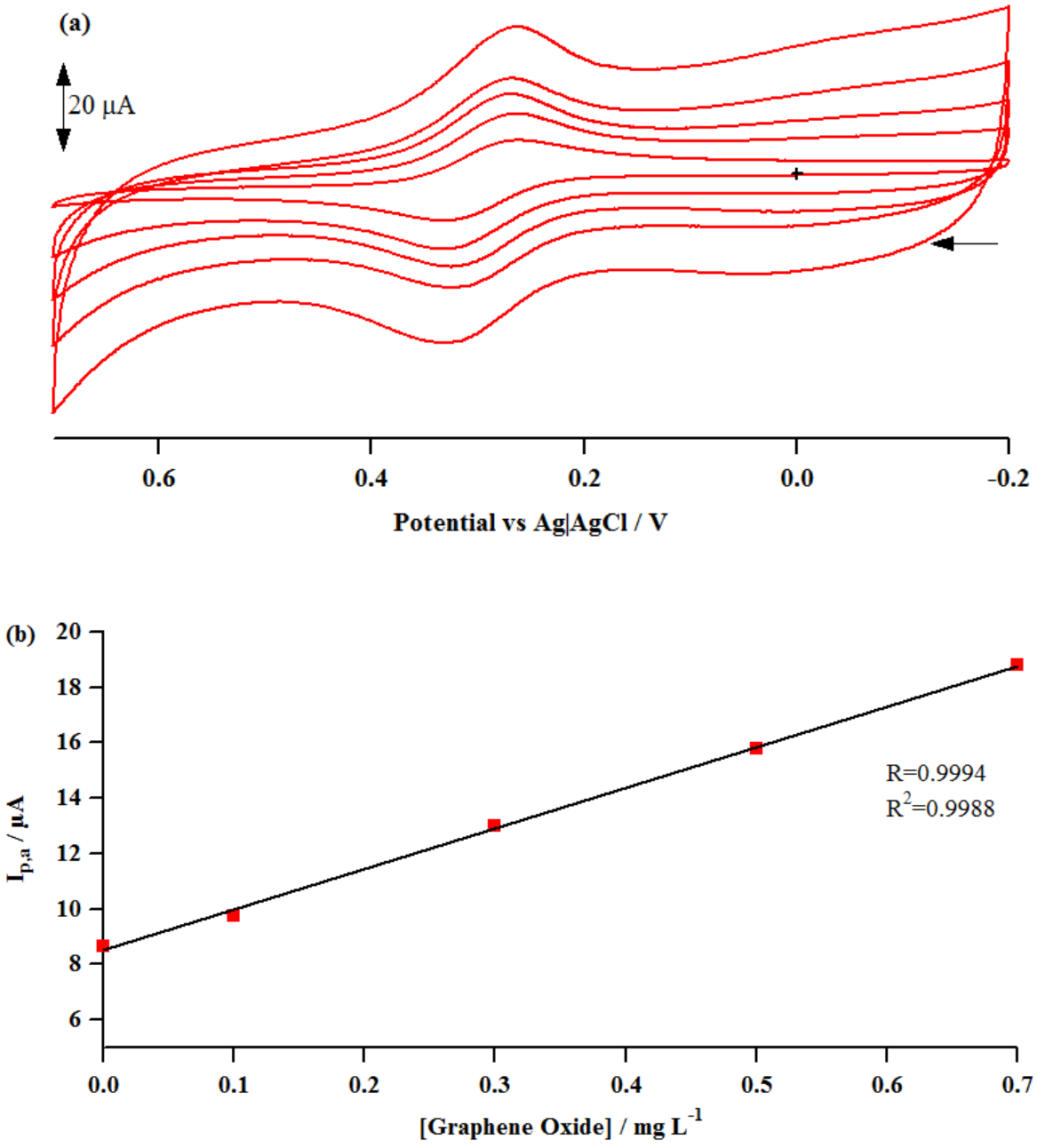

Figure 3.8 (a) Cyclic voltammetry of 1 mM ferrocenecarboxylic acid in pH 7.4 PBS with graphene oxide modified glassy carbon electrodes at a scan rate = 100 mV s^{-1}. The concentration of graphene oxide applied to glassy carbon electrode was varied from 0.1 to 0.7 mg mL^{-1}. The arrow shows the initial scan direction and the cross indicates the origin. The third scan for each concentration is shown in this figure. (b) A calibration plot of oxidation peak current versus graphene oxide concentration.

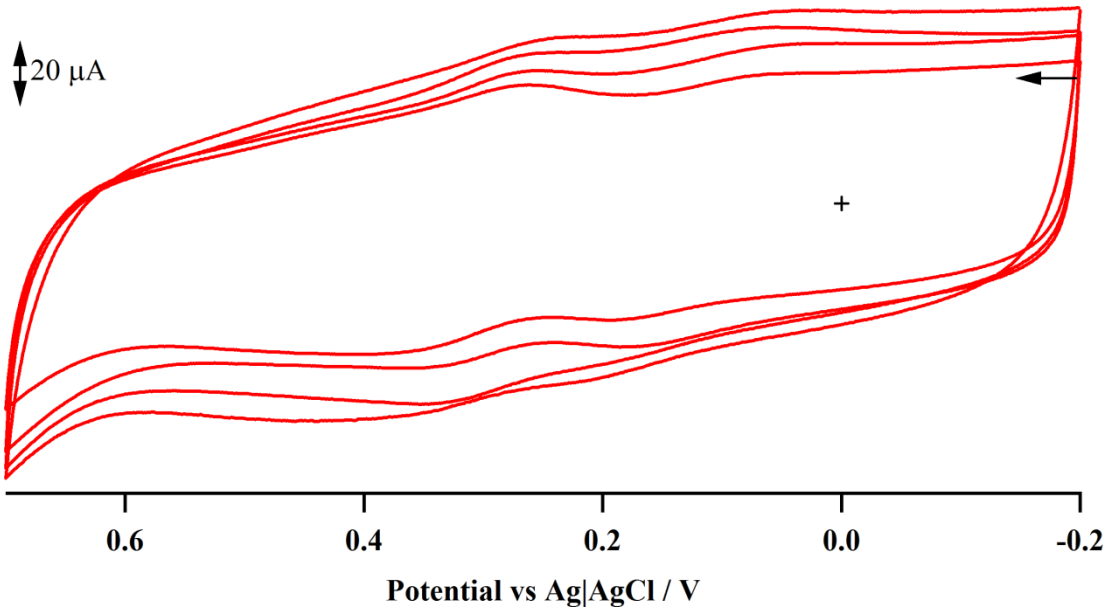

Figure 3.9 Cyclic voltammetry of 1 mM ferrocenecarboxylic acid in PH 7.4 PBS with NH_2-ERGO-glassy carbon electrodes at a scan rate = 100 mV s^{-1}. The concentration of *p*-phenylenediamine used in the diazonium reaction step was varied from 0.5 to 5.0 mM. The arrow shows the initial scan direction and the cross indicates the origin. The third scan for each concentration is shown in this figure.

Table 3.1 Experimental factors and respective levels used in a 2^3 full factorial design

Factor	Label	Factor description	Low level (-)	High level (+)
1	X_1	Concentration of graphene oxide / mg mL^{-1}	0.2	2.0
2	X_2	Concentration of *p*-phenylenediamine / mM	0.5	5.0
3	X_3	Volume of 0.04 M sodium citrate / µL	60	200

The factors and respective levels shown in Table 3.1 were used in a full 2^3 factorial design to optimise the biosensing platform. Initially, a 2^3 two-level factorial design was performed, using the oxidation peak current of 1 mM ferrocenecarboxylic acid in pH 7.4 PBS as the response signal. However, no factors or their interactions were determined to be significant. This is most likely because ferrocenecarboxylic acid is an outer sphere redox marker, which is known to display insensitivity to surface chemistry and dependent only on the distance between redox marker and electrode surface.[62] The spatial proximity the redox marker to electrode surface would have been relatively similar between conditions in the factorial design, yielding no statistically significant factors in the experiment. The full two-level factorial design based on ferrocenecarboxylic acid is shown in Table 6.1 (Supplementary Material). Inner sphere redox markers, on the other hand, for example the $Fe(CN)_6^{3-/4-}$ redox couple, are strongly affected by electrode surface modification.[18,62] In an attempt to obtain

meaningful factorial design results, a 2^3 full factorial design was repeated using the $Fe(CN)_6^{3-/4-}$ redox couple.

Cyclic voltammetric oxidation peak current of 1 mM $[Fe(CN)_6]^{3-}$ / 1 mM $[Fe(CN)_6]^{4-}$ in 0.1 M KNO_3, detected at the modified electrodes, at 100 mV s^{-1} was used as the response signal in the factorial design experiment. In addition to the factors, their interactions (X_1X_2, X_1X_3, X_2X_3 and $X_1X_2X_3$) are shown in Table 3.2. All experiments were conducted by following a randomised run order to minimise the effects of systematic errors. In Table 3.2, t_E represents the signal-to noise ratio given by Equation 3.1.[13,75]

$$t_E = \frac{\text{Effect}}{2s_p/\sqrt{n_F}} \qquad \textbf{Equation 3.1}$$

where Effect is the mean between high and low values for each factor, n_F is the number of factorial points including replication (n_F = 16) and s_p is the pooled estimate of standard deviation, evaluated by Equation 3.2.[13,75]

$$s_p^2 = \sum_{i=1}^{m} \nu_i s_i^2 \Big/ \sum_{i=1}^{m} \nu_i \qquad \textbf{Equation 3.2}$$

where m is the number of experimental conditions (m = 8), v_i is the degrees of freedom ($v_i = n_i - 1$) and s_i^2 is the variance estimate, determined by Equation 3.3.[75]

$$s^2 = (Y_1 - Y_2)^2 / 2 \qquad \textbf{Equation 3.3}$$

The oxidation peak current of 1 mM $[Fe(CN)_6]^{3-}$ / 1 mM $[Fe(CN)_6]^{4-}$ in 0.1 M KNO_3 was used as the response signal to identify significant factors and their interactions with the results presented in Table 3.2. In Table 3.2, t^* represents the critical two-tailed t value (2.31), for 8 degrees of freedom at the 95% confidence level. Factors and interactions are considered significant, and highlighted in bold font, if the absolute calculated t_E value is larger than the critical value (t^* = 2.31). The results tabulated in Table 3.2 show that X_1, X_2, X_3 and the interactions X_1X_3 and X_2X_3 are statistically significant at the 95% confidence level. These results are also graphically shown in the Pareto chart and interaction plots in Figure 3.10 and 3.11, respectively. The vertical line in the Pareto chart (Figure 3.10) shows the minimum 95% confidence interval statistically significant effect. Those factors and interactions with absolute effects greater than the vertical line were found to be statistically significant. The

factor interaction effects on detection sensitivity were shown in Figure 3.11. This figure shows a strong positive effect on the system between factors X_1 and X_3 and a strong negative effect between factors X_2 and X_3.

Table 3.2 A full 2^3 factorial design to identify significant effects and interactions at the 95% confidence level. Oxidation peak current of 1 mM $[Fe(CN)_6]^{3-}$ / 1 mM $[Fe(CN)_6]^{4-}$ in 0.1 M KNO_3 was used as the response signal. Run 9 shows centre point levels (X_1 = 1.1 mg mL^{-1}, X_2 = 2.75 mM and X_3 = 130 µL), used to statistically determine curvature in the factorial design model.

Run	X_1	X_2	X_3	X_1X_2	X_1X_3	X_2X_3	$X_1X_2X_3$	Run Order	$I_{oxidation}$ / µA	Mean / µA	Variance (s^2)
1	-	-	-	+	+	+	-	12, 8	19.3, 17.4	18.3	1.8
2	+	-	-	-	-	+	+	2, 14	17.2, 16.3	16.8	0.3
3	-	+	-	-	+	-	+	3, 13	18.3, 18.1	18.2	0.0
4	+	+	-	+	-	-	-	9, 5	20.9, 19.8	20.3	0.6
5	-	-	+	+	-	-	+	7, 10	23.0, 19.7	21.4	5.3
6	+	-	+	-	+	-	-	6, 1	25.4, 24.8	25.1	0.2
7	-	+	+	-	-	+	-	11, 15	16.7, 14.9	15.8	1.5
8	+	+	+	+	+	+	+	16, 4	17.7, 21.4	19.6	7.0
9	0	0	0	0	0	0	0	17, 18 19, 20	20.7, 19.4 17.1, 15.2	18.1	6.0
Sum product	8.09	-7.73	8.25	3.73	7.00	-14.5	-3.66				
Effect	2.02	-1.93	2.06	0.933	1.75	-3.64	-0.915				
t_E	**2.80**	**-2.67**	**2.85**	1.29	**2.42**	**-5.03**	-1.27		t*(8 degrees of freedom) = 2.31		

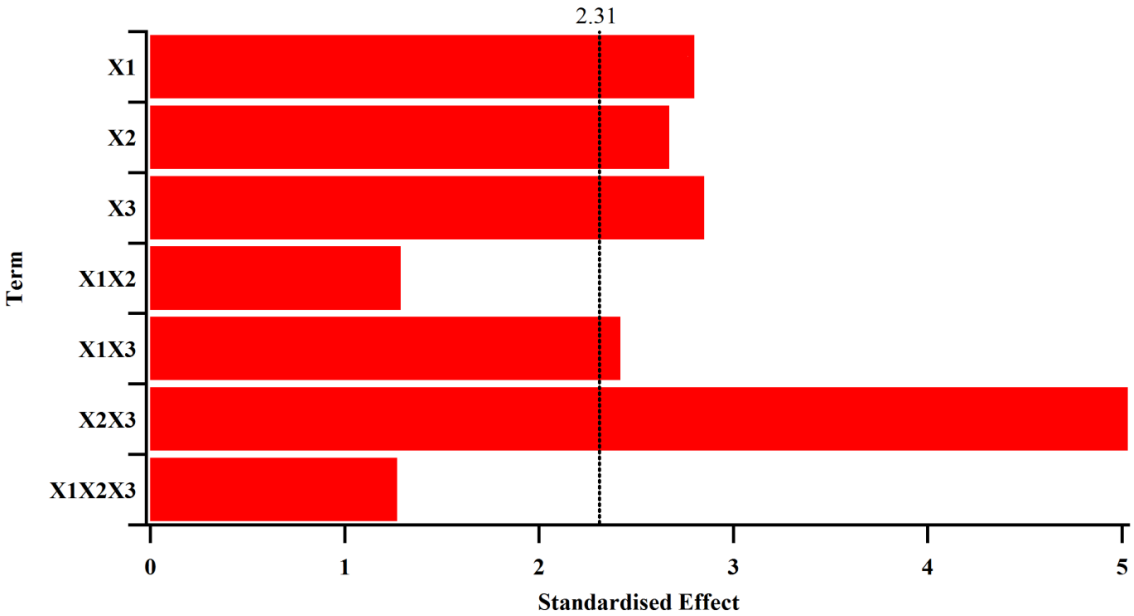

Figure 3.10 Pareto chart of the standardised effects, response is oxidation peak current of 1 mM $[Fe(CN)_6]^{3-}$ / 1 mM $[Fe(CN)_6]^{4-}$ in 0.1 M KNO_3, using the full 2^3 factorial design (presented in Table 3.2) at the 95% confidence level.

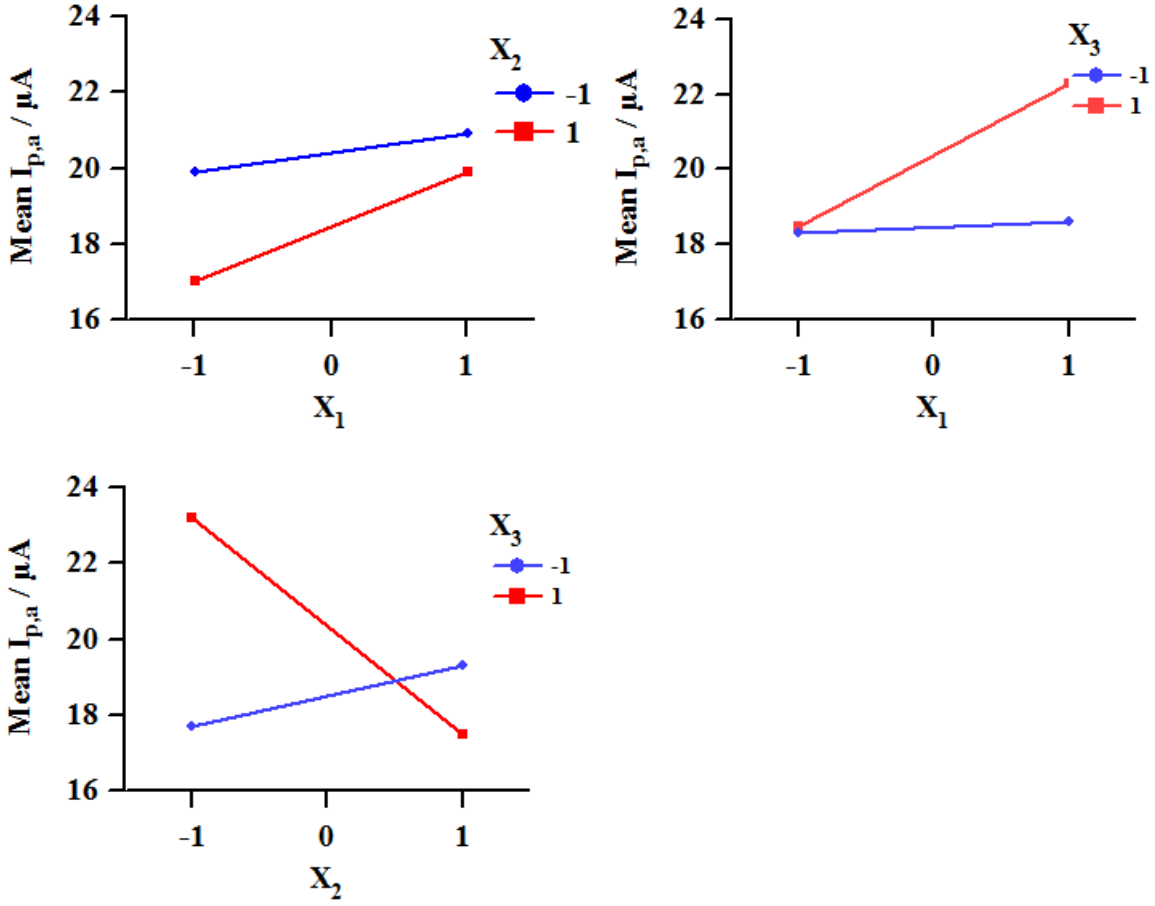

Figure 3.11 Interaction plots, response is oxidation peak current of 1 mM $[Fe(CN)_6]^{3-}$ / 1 mM $[Fe(CN)_6]^{4-}$ in 0.1 M KNO_3, using the full 2^3 factorial design (Table 3.2) at the 95% confidence level.

As expected, X_1 directly affects the surface area and electrical conductivity of the glassy carbon surface, X_2 offers sites for the formation of gold nanoparticle attachment and the negative *t*-value indicates a potential insulating effect, while X_3 directly affects the surface area of the gold nanoparticles and consequently the size of the modified electrode. The interaction X_1X_3 and X_2X_3 directly affects the charge transfer and the gold nanoparticle bonding at specific amine sites, respectively. The interactions X_1X_2 and $X_1X_2X_3$ were not significant, likely due to potential suppression of the graphene layer due to saturation of the electrode surface with the amine linker layer, minimising the synergistic properties of the two factors.

Once the significant factors and interactions have been identified, the factor values resulting in the greatest response for the optimised system were determined. To determine the optimised factor values, curvature, the difference in actual response and that predicted by a linear model, can be statistically examined. A statistical test for the significance of the

curvature in the model can be performed using the test statistic to determine curvature, shown in Equation 3.4.[75]

$$t_C = \text{Curvature} / s_C \qquad \textbf{Equation 3.4}$$

where Curvature is the difference between centre point average and factorial average values and s_C is the standard deviation of the curvature effect, calculated by Equation 3.5.[75]

$$s_C = s_p \sqrt{\frac{1}{n_C} + \frac{1}{n_F}} \qquad \textbf{Equation 3.5}$$

where s_p is the pooled estimate of standard deviation (calculated by Equation 3.2), n_C is the number of curvature points including replication (n_F = 4) and n_F is the number of factorial points including replication (n_F = 16). If no statistically significant curvature is identified, then the model can be considered linear and the optimised factor values correspond to those giving the greatest response, shown in the interaction plot in Figure 3.11.

The test statistic for curvature (t_C) was calculated using data collected using center point levels (X_1 = 1.1 mg mL^{-1}, X_2 = 2.75 mM and X_3 = 130 μL), shown in Table 3.2. The curvature test statistic was calculated to be less than the critical value, showing that there was no statistically signifcant curvature in the model at the 95% confidence level. Therefore the model can be considered linear and the optimum parameters can be selected from the interaction plot in Figure 3.11, with otimimum parameters those which give the greatest signal response. The optimum conditions for factors signficant factors X_1, X_2, X_3, and the interactions X_1X_3 and X_2X_3, were determined and used to facilitate the detection of DNA hybridisation. Here optimal values for each factor were obtained; concentration of graphene oxide (X_1) = 2.0 mg mL^{-1}, concentration of *p*-phenylenediamine (X_2) = 0.5 mM and volume of sodium citrate (X_3) = 200 μL.

Upon optimising the experimental parameters in developing the biosensing platform, the graphene oxide-4-phenyl-gold nanoparticle layer was characterised by cyclic voltammetry and EIS. Cyclic voltammetry of 1 mM $[Fe(CN)_6]^{3-}$ / 1 mM $[Fe(CN)_6]^{4-}$ in 0.1 M KNO_3 at a scan rate of 100 mV s^{-1} was performed and the results are shown in Figure 3.12. The cyclic voltammograms show a reduction peak at 0.12 ± 0.01 V and an oxidation peak at 0.26 ± 0.02 V. Upon fabrication of ERGO-glassy carbon electrodes the baseline corrected peak current decreased by 9.7%, NH_2-ERGO-glassy carbon electrodes decreased by 47.2%

and AuNP-Ph ERGO-glassy carbon electrodes increased by 0.3%, all relative to that at the glassy carbon electrode. This showed that the final biosensor platform design exhibited a synergistic effect over the individual electrode modifications, increasing the magnitude of the peak current measured. A slight increase in the sensitivity of the biosensing platform, determined by peak current, was observed following modification; however selectivity was introduced offering gold nanoparticle sites for covalent attachment of thiol-labelled ssDNA probes.

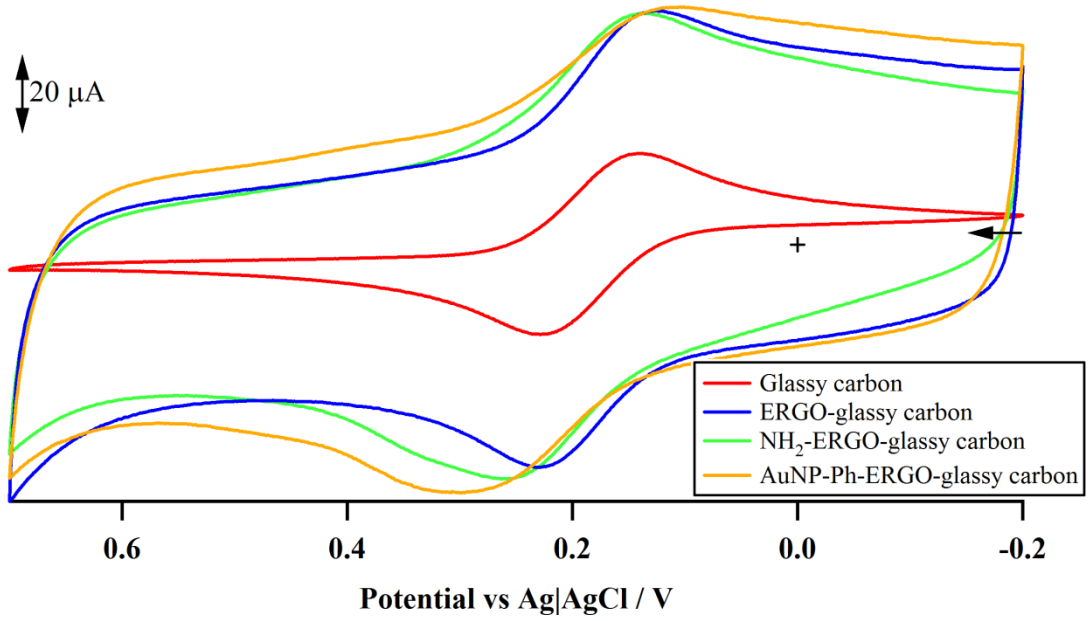

Figure 3.12 Cyclic voltammetry of 1 mM $[Fe(CN)_6]^{3-}$ / 1 mM $[Fe(CN)_6]^{4-}$ in 0.1 M KNO_3 at the optimised biosensor platform; scan rate = 100 mV s^{-1}. The arrow shows the initial scan direction and the cross indicates the origin. The third scan for each modified electrode is shown in this figure.

In addition to voltammetric characterisation of a modified electrode, EIS offers important information regarding the capacitance and charge transfer kinetics. The biosensing platform in this work was also characterised by EIS to study the change in capacitance at the electrode surface and ability of the electrodes to transfer charge from surrounding molecules, following the modification with different surface layers, using 1 mM $Fe(CN)_6^{3-}$ / 1 mM $Fe(CN)_6^{4-}$ in 0.1 M KNO_3 supporting electrolyte as the redox marker. The DC potential applied was that with the lowest resistance, corresponding to the half-wave potential determined by cyclic voltammetry, independently for each electrode. An alternating potential of 10 mV in amplitude in the frequency range of 10 kHz to 0.1 Hz, spaced logarithmically, was superimposed on the applied DC potential. The resulting imaginary impedance (-Z'') versus real impedance (Z') Nyquist plot at the modified electrodes, is presented in Figure 3.13.

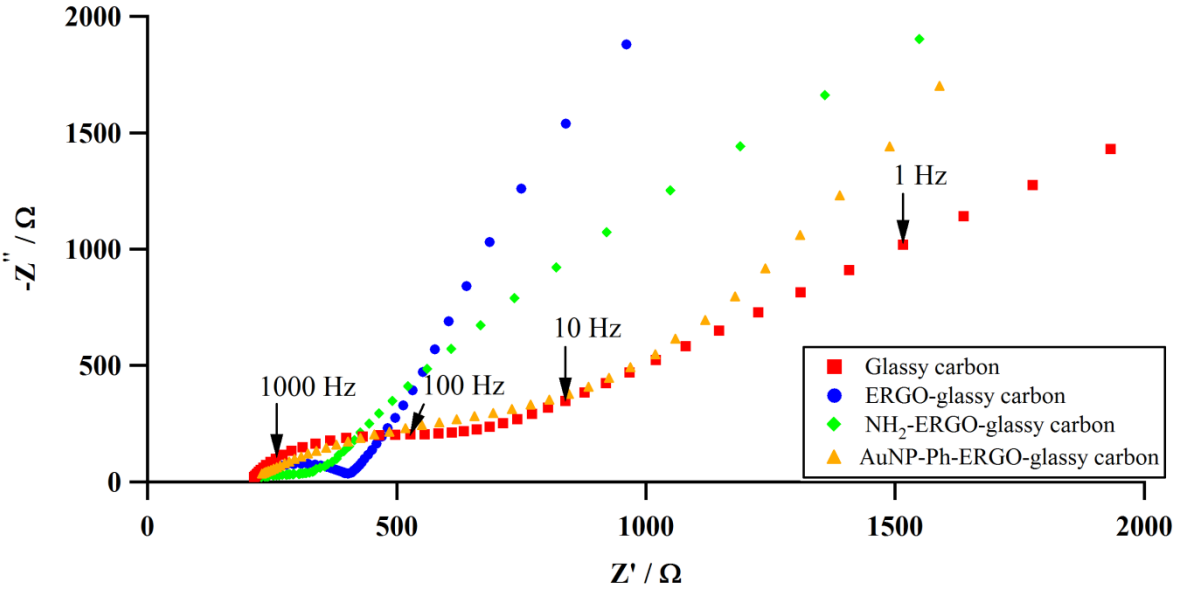

Figure 3.13 Nyquist plots for optimised, modified electrodes at each stage of the biosensor platform fabrication in 1 mM $[Fe(CN)_6]^{3-}$ / 1 mM $[Fe(CN)_6]^{4-}$ in 0.1 M KNO_3 origin. Applied DC potentials were determined from the half wave potential determined from cyclic voltammetry and an AC signal (amplitude 10 mV) was applied in the frequency range 10 kHz to 0.1 Hz.

In Figure 3.13, each of the traces representing different electrode modification layers exhibits a semicircle in the high frequency region, followed by a linear response in the low frequency region. In the high frequency region, the electrolyte solution resistance (R_s) corresponds to the offset of the semicircle on the real impedance axis, while the diameter of the semicircle represents the electron transfer resistance (R_{et}). In the low frequency region, the linear response arose from the diffusion process of the electrode reaction, known as the Warburg impedance (Z_w). A Randles circuit can be used to represent an electrode solution interface and fit experimental data. The Randles circuit used for data fitting is shown in Figure 3.14. It consists of a constant phase element (CPE), which incorporates the double layer capacitance, which is in a parallel circuit to both R_{et} and Z_w and in a series arrangement to R_s. Experimental EIS data were fitted to the Randles circuit in Figure 3.14 and mean values with 95% confidence intervals are tabulated in Table 3.3. Both R_s and Z_w are independent of the electrode and are expected to remain constant for each electrode modification tested and R_{et} and CPE are dependent on the electrode-redox marker interaction, making these values useful in comparing the electrochemical properties of modified electrodes.

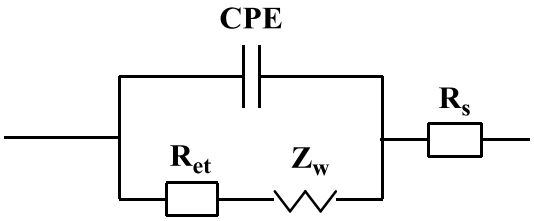

Figure 3.14 Randles circuit model used for EIS data fitting.

Table 3.3 Summary of mean EIS simulation results, with 95% confidence intervals (CI), obtained at each stage of fabrication of optimised biosensing platform. Three different modified electrodes were analysed with each modification.

Electrode	R_s / Ω	CI / Ω	R_{et} / Ω	CI / Ω	CPE / μF	CI / μF	Z_w / Ω	CI / Ω
Bare glassy carbon	222	10	306	47	0.5	0.1	3.11×10^{-4}	6.7×10^{-6}
ERGO-glassy carbon	199	20	45.1	40	1.5	0.5	2.00×10^{-3}	1.4×10^{-6}
NH_2-ERGO-glassy carbon	228	10	62.2	2	1.4	0.4	8.72×10^{-4}	2.5×10^{-4}
AuNP-Ph-ERGO-glassy carbon	232	30	213	71	2.1	1.9	2.39×10^{-4}	1.8×10^{-4}

The fitted mean EIS results in Table 3.3 show consistent values of R_s and Z_w obtained, which is expected as R_s and Z_w are independent of the electrode surface modification. However a substantial difference in the R_{et} values is observed due to the respective electrode modifications. ERGO-glassy carbon exhibits the lowest electron transfer resistance of 45.1 ± 40 Ω, which is expected due to the excellent electrical conductivity of graphene.[39] Despite the insulating nature of the surface aryl amine groups, NH_2-ERGO-glassy carbon electrodes display an R_{et} of 62.2 ± 2 Ω, similar to that of the graphene modified electrodes, likely due to good conductivity of graphene dominating the charge transfer event. Finally, the AuNP-Ph-ERGO-glassy carbon electrodes have a higher R_{et} value, 213 ± 71 Ω which can be explained by the either electrostatic repulsion of $Fe(CN)_6^{3-/4-}$ with the negatively charged citrate capping agent or the additional surface layers of the biosensor platform reducing the electron transfer from the redox site to the electrode surface. These R_{et} results are in agreement with the corresponding cyclic voltammogram data (Figure 3.12), with larger cyclic voltammogram peak separation observed for the modified electrodes with larger R_{et} values from EIS. It should be noted that the 95% confidence intervals of R_{et} values are relatively large as a result of different electrodes being analysed and inherent differences in the surface coverage.

Finally, the double layer capacitance (estimated from CPE), showed an increase in capacitance with additional surface layers. The AuNP-Ph-ERGO-glassy carbon electrodes displayed a capacitance four times greater than the bare glassy carbon electrodes. This increased capacitance is also observed in the large separation between forward and reverse scans in cyclic voltammetry (Figure 3.12) and is a result of an increasing number of surface layers on the developed biosensing platform.

3.4 Detection of DNA hybridisation

Following the development and optimisation of the approach to fabricate the electrochemical DNA biosensor platform, a ssDNA sequence before hybridisation was next immobilised on the biosensor surface to hybridise with the complementary sequence and signal amplification with Zr(IV). The detection of biologically important 19 base pair DNA sequences, related to the BRCA1 protein, were analysed as a model biological analyte. The BRCA1 protein encoding gene is of biological importance as mutations in the *BRCA*1 gene have been reported to be involved in breast cancer due to the introduction of stop codons.[1,14,30,31] The capture probe, a thiol-labelled 19 oligonucleotide sequence, complementary to the *BRCA1* gene target was reduced with TCEP, denatured by heating and covalently bonded to gold nanoparticles on the modified electrode surface. Hybridisation was then promoted by incubating the ssDNA-AuNP-Ph-ERGO-glassy carbon electrode in an appropriate DNA target solution for 15 min, followed by incubation in the oxygen-attracting Zr(IV) for a further 15 min.

Initially, the ssDNA modified electrode was incubated in a 3 µM solution of the complementary target solution. Cyclic voltammetry of the negatively charged, inner sphere redox couple, $Fe(CN)_6^{3-/4-}$, was used to study the electrochemical characteristics of the hybridised electrochemical DNA biosensor and the results obtained are shown in Figure 3.15. Initially the cyclic voltammogram for the biosensor platform showed an oxidation peak and reduction peak at 0.34 ± 0.04 V and 0.00 ± 0.06 V, respectively. Suppression of the current peaks, to a peak current indistinguishable from the baseline, is observed following immobilisation of the negatively charged ssDNA probe. This can be attributed to the repulsion of the negatively $Fe(CN)_6^{3-/4-}$ backbone through electrostatic repulsion with the negatively charged phosphate backbone of the ssDNA sequence. Upon hybridisation with the complementary target sequence, a further decrease in the peak is observed, due to an increased number of phosphate groups in the DNA duplex and an increased negative charge.

As a result of the electrostatic repulsion, the accessibility of the analyte to the electrode surface is decreased, resulting in a loss of peak current at the oxidation and reduction peak currents of 0.34 ± 0.04 V and 0.00 ± 0.06 V, respectively. This preliminary DNA hybridisation experiment shows the successful attachment of ssDNA probe on the biosensing surface and successful hybridisation with the target DNA sequence.

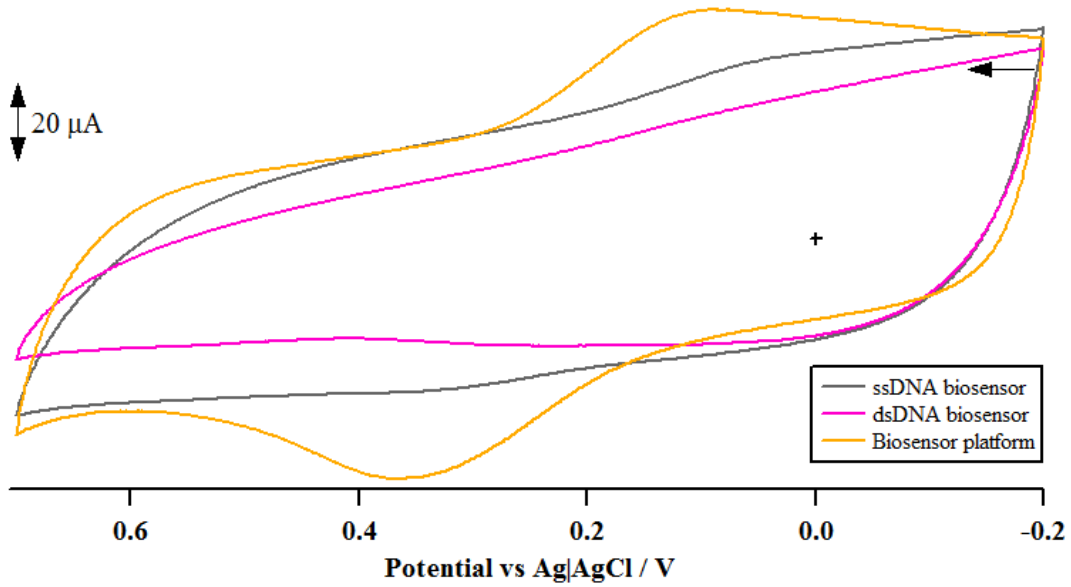

Figure 3.15 Cyclic voltammograms of 1 mM $[Fe(CN)_6]^{3-}$ / 1 mM $[Fe(CN)_6]^{4-}$ in 0.1 M KNO_3 at the optimised biosensor platform, ssDNA biosensor and dsDNA biosensor; scan rate = 100 mV s^{-1}. The arrow shows the initial scan direction and the cross indicates the origin. The third scan for each sensor is shown in this figure.

Next, the inorganic Zr(IV) ion was incorporated in the DNA duplex to attract an oxygen-containing redox marker, ferrocenecarboxylic acid, to the electrode surface.[13,33] To confirm the successful incorporation into the DNA duplex and enhancement of electrochemically detected signal, cyclic voltammetry of 1 mM ferrocenecarboxylic acid pH 7.4, scanning potential from -0.2 V to 0.7 V, was performed following incubation in 3 µM complementary DNA target and Zr(IV) for 15 min each. Overlaid cyclic voltammograms obtained at the glassy carbon electrode, optimised biosensing platform, Zr(IV)-ssDNA-AuNP-Ph-ERGO-glassy carbon electrode and Zr(IV)-dsDNA-AuNP-Ph-ERGO-glassy carbon electrode are presented in Figure 3.16. Initially the cyclic voltammogram obtained at the biosensor platform showed an oxidation peak and reduction peak at 0.34 ± 0.01 V and 0.24 ± 0.01V, respectively. Upon immobilisation of the ssDNA probe and incubation in Zr(IV), an oxidation peak current decrease of 22% was observed. Finally hybridisation with 3 µM

target, the oxidation peak current increased from the ssDNA probe modified electrode and exhibited an oxidation peak current decrease of 12% decrease from the DNA platform. This increased peak current of the Zr(IV)-dsDNA-AuNP-Ph-ERGO-glassy carbon electrode over the corresponding precursor, Zr(IV)-ssDNA-AuNP-Ph-ERGO-glassy carbon electrode, can be accounted for by increased Zr(IV) being incorporated into the DNA duplex which electrostatically attracted ferrocenecarboxylic acid to the electrode surface for oxidation to occur. This increased electrochemical signal was the basis for DNA hybridisation detection using the developed electrochemical DNA biosensor.

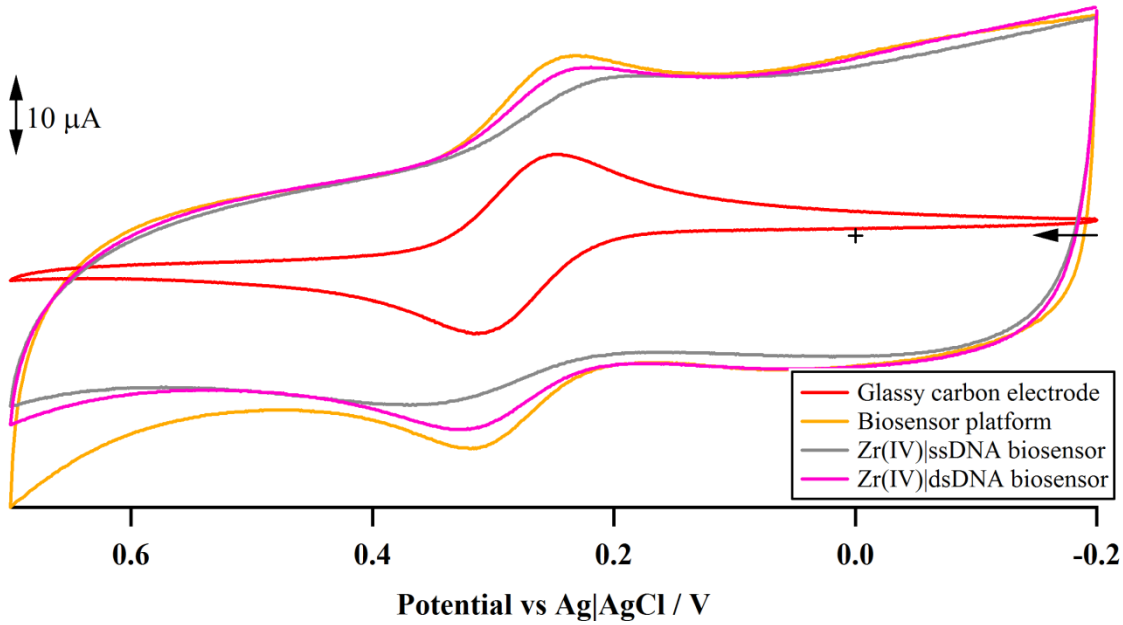

Figure 3.16 Cyclic voltammograms of 1 mM ferrocenecarboxylic acid in pH 7.4 PBS at glassy carbon electrodes, the optimised biosensor platform, Zr(IV)|ssDNA biosensor and hybridisation in 3 µM target solution to produce the Zr(IV)|dsDNA biosensor; scan rate = 100 mV s^{-1}. The arrow shows the initial scan direction and the cross indicates the origin. The third scan for each voltammogram is shown in this figure.

The sensitivity of electrochemical DNA biosensors is a critical element of a DNA biosensor and is one of the measures of analytical performance. In this work, square wave voltammetry was used to determine the analytical performance of the developed biosensor while minimising the contribution of non-Faradaic, background current. ssDNA-AuNP-Ph-ERGO-glassy carbon electrodes were incubated in target DNA solutions of concentrations ranging from 10 to 100 nM. Hybridisation was detected using square wave voltammetry of 1 mM ferrocenecarboxylic acid in pH 7.4 PBS, between 0 and 0.6 V. This was assessed by evaluating $\Delta I_{p,a}$, the net oxidation peak current detected (*i.e.* the ssDNA biosensor signal

subtracted from the dsDNA biosensor signal). Figure 3.17 (a) shows the square wave voltammograms obtained following incubation in target DNA solutions of concentration 10, 20, 50 and 100 nM. Here, the peak at 0.28 V was observed to increase when the concentration of target sequence was increased from 10 to 100 nM. A calibration plot based on $\Delta I_{p,a}$ is depicted in Figure 3.17 (b), shows a linear relationship in with concentration of target DNA solution (correlation coefficient of 0.9995 (N = 4), which was found to be statistically significant at the 95% confidence level), which can be expressed as:

$$\Delta I_{p,c} = (0.068 \pm 0.006\ \mu\text{A nM}^{-1})[DNA_{\text{target}}] + (0.085 \pm 0.37\ \mu\text{A}) \quad \textbf{Equation 3.6}$$

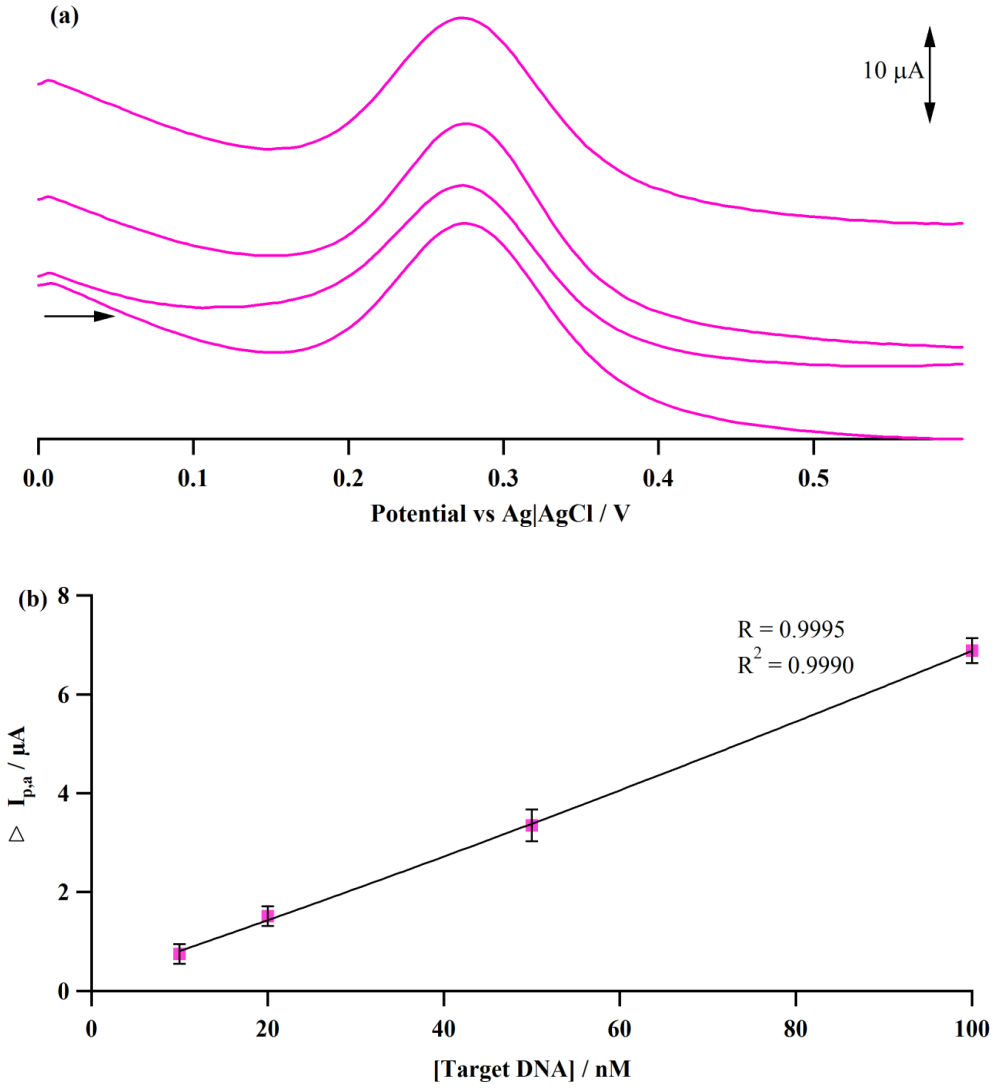

Figure 3.17 (a) Square wave voltammograms of 1 mM ferrocenecarboxylic acid in pH 7.4 PBS following 15 min incubation of the optimised ssDNA-biosensor in the complementary target DNA solutions of concentration 10, 20, 50 and 100 nM. A y-offset was applied to raw current. A scan rate of 100 mV s^{-1}, frequency of 25 Hz, a pulse height of 2 mV and amplitude of 25 mV was used. (b) A calibration plot based on $\Delta I_{p,a}$ from square wave voltammograms shown in (a). Error bars represent the 95% confidence intervals.

Based on a signal-to-noise ratio of 3, the detection limit was estimated to be 4.6 nM. Additionally the dynamic range of the electrochemical DNA biosensor was found to be between 15.5 nM and 100 nM. Finally, the reproducibility of the developed biosensor can be evaluated by a relative standard deviation of 4% in the responses of three different sensors (prepared in an identical manner) to 50 nM of target analyte. The repeatability of the developed electrochemical DNA biosensor was not determined in this work as the developed biosensors are non-reusable, due to irreversible hybridisation with a complementary DNA sequence forming a stable DNA duplex.

The selectivity of fabricated electrochemical DNA biosensors is paramount in the development of sensors. In the application to detection of *BRCA1* related gene sequences in this work, the ability to differentially detect different DNA sequences with single base mutations is essential for the potential use in diagnostics. To examine this feature of the fabricated biosensor, a label-free experiment comparing the detection signals of different sequences was performed. ssDNA-AuNP-Ph-ERGO-glassy carbon electrodes were prepared using optimised conditions and electrodes were incubated in 30 μM of target, 1-mismatch, 3-mismatch and non-complementary sequences, followed by incubation in the oxygen-attracting Zr(IV). Electrochemical detection was performed using cyclic voltammetry from -0.2 V to 0.7 V in the presence of the oxygen-containing ferrocenecarboxylic acid in pH 7.4 PBS and the performance of the electrodes was determined by comparing the difference in oxidation peak current ($\Delta I_{p,a}$) before and after hybridisation. Three biosensors were analysed by cyclic voltammetry after hybridisation in each target DNA sequence, shown in Figure 3.18. An average $\Delta I_{p,a}$ of 3.4 ± 0.9, 2.2 ± 0.4, 1.5 ± 0.2 and 0.6 ± 0.2 was estimated for the target, 1-mismatch, 3-mismatch and non-complementary sequences, respectively. The signal of the target DNA was 35%, 56% and 82% greater than the 1-mismatch, 3-mismatch and non-complementary sequences, respectively. As expected, the current change signal obtained from detection of the non-complementary signal was insignificant in comparison to the target sequence, due to non-specific hybridisation. The results also show successful differential differentiation between target DNA sequences and sequences containing SNPs, which is a useful property in the detection of *BRCA1* gene sequences.

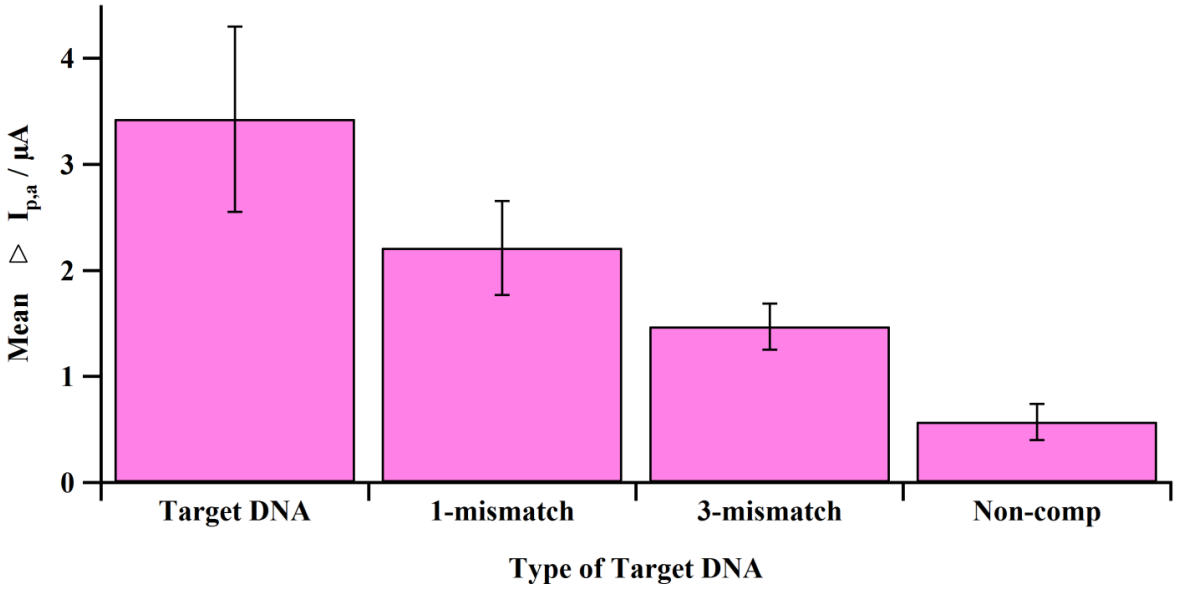

Figure 3.18 Histogram showing the $\Delta I_{p,a}$ of 1 mM ferrocenecarboxylic acid in pH 7.4 PBS, determined from cyclic voltammetry with a scan rate of 100 mV s^{-1}, following 15 min incubation of the optimised electrochemical DNA biosensor in 30 µM solutions of the target, 1-mismatch, 3-mismatch and a non-complementary DNA sequence, before incubation in 10 mM Zr(IV) solution for 15 min.

In this work, a glassy carbon electrode was modified based on factorial design optimised graphene, and amine linker and gold nanoparticles to produce a biosensing platform. A ssDNA probe was covalently attached by gold-thiol bonding and Zr(IV) was incorporated to electrostatically attract ferrocenecarboxylic to the electrode surface. A comparison of the analytical performance of our biosensor for detection of similar, label-free electrochemical DNA biosensors is tabulated in Table 3.4. The detection limit compared favourably with many reported biosensors. However while the detection limit is higher than that reported by Wipawakarn *et al.*[13] and Rasheed and Sandhyarani,[30] the electrochemical DNA biosensor developed in this work was demonstrated to differentiate between sequences down to single base mutations. Additionally, our biosensor exhibited a greater reproducibility, estimated by relative standard deviation (4%) than the diazonium-based biosensor produced by Revenga-Parra *et al.*[49] (7%). The ability to differentially detect single base mutations is of paramount importance in detection of genetic mutations and offers the possible for use of the biosensor as a potential diagnostic tool. The increased selectivity of the developed biosensor could be associated with the approach used to incorporate gold nanoparticles in the biosensor design. Gold nanoparticles were incorporated into the biosensor through covalent C-Au bonds rather than the more commonly reported NH-Au bonds, due to superior the bond strength of the gold-carbide bond.[36] As a result, the stability of the biosensor will be enhanced. However,

while increasing the stability, this method of gold nanoparticle attachment has been reported to yield a much lower density of gold nanoparticles than compared with other NH-Au covalent bonding.[36] We hypothesise that due to the lower density of immobilised gold, it would be expected that fewer ssDNA probe sequences could be attached to the biosensor surface, reducing the chance of non-specific DNA hybridisation occurring due to limited steric effects. Based on the reasonable sensitivity and excellent selectivity, the developed electrochemical DNA biosensor exhibits favourable properties for biosensing. While *BRCA1* gene related sequences were used to characterise the performance of this electrochemical DNA biosensor, the biosensor could similarly be used for detection of any thiol-labelled DNA sequences.

Table 3.4 A comparison of different types of similar, label-free, recently reported electrochemical DNA biosensors, including the present work.

Reference	Biosensor design	Detection technique	Detection limit
Li *et al.*[1]	Carboxylic acid functionalised, carbon nanotube-based screen printed carbon electrodes.	Differential pulse voltammetry	0.4 μM
Wipawakarn *et al.*[13]	Carbon nanofibre, chitosan, glutaraldehyde modified glassy carbon electrode. dsDNA incubated in Zr(IV).	Differential pulse voltammetry	88 pM
Revenga-Parra *et al.*[49]	DNA immobilised through covalent bonding the diazonium groups on screen printed carbon electrodes.	Differential pulse voltammetry	4.7 nM
Rasheed and Sandhyarani[30]	Sandwich-type hybridisation on graphene-modified glassy carbon electrodes. Signal enhancement with gold nanoparticles.	Chronoamperometry	1 fM
This work	Graphene, aryl diazonium linker, gold nanoparticles modified glassy carbon electrode. dsDNA incubated in Zr(IV).	Square wave voltammetry	4.6 nM

Chapter 4

CONCLUSIONS

4.1 Concluding remarks

Electrochemical DNA biosensors are important sensors for monitoring DNA hybridisation efficiency, with potential applications including monitoring of pharmaceutical agent effectiveness,[4] environmental analysis[6] and as a diagnostic tool for genetic-based conditions.[28] One of the common approaches to developing electrochemical DNA biosensors involves immobilisation of a ssDNA probe as the biological recognition element, to impart selectivity, on an electrochemical transducing element, which generally affects sensitivity. Different approaches to immobilisation strategies of the biorecognition element and modification of the transducing element have been reported in an attempt to increase sensitivity and selectivity, as described in Section 1.2. While many electrochemical DNA biosensors have been fabricated, few have been reported to display both high sensitivity and selectivity. For example, our laboratory recently reported an electrochemical biosensor with a detection limit of 88 pM for a target DNA sequence, however selectivity to single-base mutations was not demonstrated.[13]

In this work, we have developed a label-free electrochemical DNA biosensor for the *in vitro* monitoring of DNA hybridisation using gene sequences related to BRCA1, a biologically important protein involved in breast cancer, as model biological analytes. The electrochemical DNA biosensor consisted of a nanomaterial modified glassy carbon electrode, including electrochemically reduced graphene oxide, an amine linking layer and gold nanomaterials, which were incorporated through relatively strong C-Au bonds utilising a diazonium reaction and electrochemical reduction. Unlike many of the reported approaches for parameter optimisation, a two-level factorial design was performed to identify significant factors and their interactions and to identify the optimum values for each factor. A thiol-labelled ssDNA probe sequence was immobilised on the electrode surface to undergo hybridisation with a *BRCA1* related gene sequence. Finally Zr(IV) was incorporated into the DNA duplex to amplify the detection signal.

Following method development, a full two-level factorial design was performed to identify significant factors and their interactions to form a modified transducing surface as the basis of the electrochemical DNA biosensor. The importance of inner and outer sphere redox markers was identified and an inner sphere redox marker was used to show that each of the primary factors concentration of graphene oxide immobilised on the electrode surface, concentration of *p*-phenylenediamine used in anchoring the amine layer through diazonium chemistry and the volume of sodium citrate solution used to generate gold nanoparticles were statistically significant at the 95% confidence level, along with some of their two-way interactions. Based on the 2^3 factorial design, an anchoring layer of optimal composition of 2.0 mg mL^{-1} graphene oxide, 0.5 mM *p*-phenylenediamine and 200 μL sodium citrate reducing agent was employed. Cyclic voltammetry showed that the optimised biosensing platform exhibited a 0.3% sensitivity increase over the bare glassy carbon electrode and importantly selectivity was imparted through surface gold nanoparticles.

A 19 base ssDNA probe was immobilised to the optimised DNA sensing platform, followed by hybridisation with its complementary *BRCA1* gene target and incorporation of positive Zr(IV) into the negative phosphate backbone of hybridised DNA to enhance the detection signal. The degree of hybridisation was assessed by a label-free electrochemical approach, with the net change in ferrocenecarboxylic acid oxidation peak current determined. The biosensor was shown to exhibit excellent sensitivity by electrochemical detection when treated with 30 μM of target sequences, with single base mutations differentiated from the target sequences. The analytical performance of the developed biosensor was also examined using the *BRCA1* gene target sequence. A linear dynamic range between 15.5 and 100 nM of the DNA target, with a detection limit (based on a signal-to-noise ratio of 3) of 4.6 nM achieved. The sensitivity of the sensor was comparable to recently reported electrochemical DNA biosensors[1,13,49] and excellent selectivity was demonstrated.

In summary, an electrochemical DNA biosensor was developed consisting of electrochemically reduced graphene oxide, an amine linking layer and gold nanoparticles on a glassy carbon electrode. A thiol-labelled DNA probe was immobilised on the electrode surface which hybridised with a *BRCA1* related gene sequence and Zr(IV) was incorporated to increase the detected signal intensity. The biosensor displayed reasonable sensitivity and excellent sensitivity when a 19 base *BRCA1* related model biological analyte was detected.

4.2 Future directions

In this work, the transducing element consisted of reusable, nanomaterial modified, macro-based glassy carbon electrodes for *in vitro* detection of genetic mutations related to the BRCA1 protein. However in biosensing for *in vivo* diagnostic applications, small and disposable electrochemical DNA biosensors would be advantageous. Therefore, a possible future direction for this work is to apply the biosensor fabrication procedure to screen-printed electrodes for *in vivo* applications of the biosensor as a potential biomarker for breast cancer, or similarly, other genetic-based diseases. Screen-printed electrodes are low-cost, disposable and highly reproducible electrodes which have been reported in DNA biosensing applications.[49,76]

Another area of recent interest in electrochemical DNA biosensor development is orientated around the use of diamond electrodes and nanodiamonds as electrode materials.[22] Diamond electrodes consist of an sp^3 carbon lattice and are ideal materials for biosensing due to excellent chemical and electrochemical stability, a larger potential window and lower background currents than other electrode materials.[33,77] However, despite the advantageous properties of bulk diamond electrodes, high costs currently limit the incorporation of diamond electrodes to biosensing applications. To expand the repertoire of biosensing electrode surfaces, a pseudo, diamond-like surface to function as the transducing element for an electrochemical DNA biosensor could potentially be generated by the reduction of oxygen groups on the surface of a glassy carbon electrode to form a hydrophobic, largely sp^3 hybridised carbon electrode surface.

To facilitate reduction of oxygen groups on a glassy carbon electrode, a reduction method using silane-based reducing agents could be used.[78] The reaction scheme is shown in Supplementary Material Figure 6.2 (a) with a series of reduction reactions, including the reduction of a primary alcohol, ketone and carboxylic acid using *n*-butylsilane as the reducing agent and catalysed by the Lewis acid tris(pentafluorophenyl)borane, to form silyl ethers and alkanes. This reduction reaction could potentially be applied to a glassy carbon electrode surface, which comprises of hydroxyl, ketone, carboxylic and quinonic functional groups.[62] By using the silane reduction method, the various oxygen-containing functional groups could be modified to generate a hydrophobic surface, largely containing sp^3 hybridised carbon atoms, to generate a pseudo diamond electrode surface. This proposal is shown in Figure 6.2

(b, Supplementary Material), with potential oxygen containing surface groups on a glassy carbon electrode reduced using the silane-based reduction method.

A second future of this work could involve development of another label-free electrochemical DNA biosensor, based on a diamond-like electrode substrate surface. Figure 6.3 (Supplementary Material) shows the structure of the proposed diamond-like electrode surface, obtained using the silane-based reduction reaction, UV-catalysed alkene chemistry and a gold nanoparticle scaffold. In an analogous manner to the glassy carbon based biosensor already developed in this work, probe ssDNA sequences will be immobilised using thiol-gold covalent bonding and Zr(IV) will be incorporated into the hybridised dsDNA to amplify detection of the electrochemical signal. By developing a second electrochemical DNA biosensor, the scope of potential applications of DNA hybridisation monitoring could be greatly enhanced.

In an application perspective, the developed electrochemical DNA biosensor can be used to directly study interactions between, for example, chemotherapy-based drugs and a particular DNA sequence.[79] The nature of DNA-adduct interactions are typically characterised by a combination of biological and chemical assays including electrophoresis, nuclear magnetic resonance, mass spectrometry and chromatography, however due to the simplicity, reliability and small quantity of sample required, electrochemical DNA biosensors offer alternative characterisation opportunities.[79] Therefore the scope of applications of the developed biosensor could be diversified from the detection of biologically important DNA sequences, reported in this work, to characterisation of specific DNA-adduct interactions.

Chapter 5

REFERENCE LIST

5.1 Reference List

(1) Li, C.-Z.; Karadeniz, H.; Canavar, E.; Erdem, A. *Electrochim. Acta* **2012**, *82*, 137-142.
(2) Kaur, B.; Srivastava, R. *Electrochim. Acta* **2014**, *133*, 428-439.
(3) Garrett, R.; Grisham, C. *Biochemistry*, 3rd ed.; Thomson Learning: United States of America, 2005.
(4) Nawaz, H.; Rauf, S.; Akhtar, K.; Khalid, A. M. *Anal. Biochem.* **2006**, *354*, 28-34.
(5) Benvidi, A.; Rajabzadeh, N.; Mazloum-Ardakani, M.; Heidari, M. M.; Mulchandani, A. *Biosens. Bioelectron.* **2014**, *58*, 145-152.
(6) Sha, Q.; Forstner, M. R.; Bonner, T. H.; Hahn, D. *J. Aquat. Anim. Health* **2013**, *25*, 184-190.
(7) Hao, Y.; Zhou, B.; Wang, F.; Li, J.; Deng, L.; Liu, Y.-N. *Biosens. Bioelectron.* **2014**, *52*, 422-426.
(8) Ligaj, M.; Tichoniuk, M.; Gwiazdowska, D.; Filipiak, M. *Electrochim. Acta* **2014**, *128*, 67-74.
(9) Xu, W.; Xue, X.; Li, T.; Zeng, H.; Liu, X. *Angew. Chem., Int. Ed.* **2009**, *48*, 6849-6852.
(10) Sun, Y.; Xu, Y.; Chambon, P. *Nucleic Acids Res.* **1982**, *10*, 5753-5763.
(11) Xiao, Y.; Plakos, K. J.; Lou, X.; White, R. J.; Qian, J.; Plaxco, K. W.; Soh, H. T. *Angew. Chem.* **2009**, *121*, 4418-4422.
(12) Liu, P.; Li, X.; Greenspoon, S. A.; Scherer, J. R.; Mathies, R. A. *Lab Chip* **2011**, *11*, 1041-1048.
(13) Wipawakarn, P.; Ju, H.; Wong, D. K. *Anal. Bioanal. Chem.* **2012**, *402*, 2817-2826.
(14) Mohan, S.; Nigam, P.; Kundu, S.; Prakash, R. *Analyst* **2010**, *135*, 2887-2893.
(15) Kong, R.-M.; Song, Z.-L.; Meng, H.-M.; Zhang, X.-B.; Shen, G.-L.; Yu, R.-Q. *Biosens. Bioelectron.* **2014**, *54*, 442-447.
(16) Lin, C.; Wu, Y.; Luo, F.; Chen, D.; Chen, X. *Biosens. Bioelectron.* **2014**, *59*, 365-369.
(17) Shi, A.; Wang, J.; Han, X.; Fang, X.; Zhang, Y. *Sens. Actuators, B* **2014**, *200*, 206-212.
(18) Giovanni, M.; Bonanni, A.; Pumera, M. *Analyst* **2012**, *137*, 580-583.
(19) Zhang, Y.; Zhang, K.; Ma, H. *Am. J. Biomed. Sci.* **2009**, *1*, 115-125.
(20) Clark, L. C.; Lyons, C. *Ann. N. Y. Acad. Sci.* **1962**, *102*, 29-45.
(21) Prieto-Simón, B.; Saint, C.; Voelcker, N. H. *Anal. Chem.* **2013**, *86*, 1422-1429.
(22) Zhang, W.; Patel, K.; Schexnider, A.; Banu, S.; Radadia, A. D. *ACS Nano* **2014**, *8*, 1419-1428.
(23) Shen, G.; Hu, X.; Song, S. *J. Electroanal. Chem.* **2014**, *717-718*, 172-176.
(24) Liu, X.; Zhang, J.; Liu, S.; Zhang, Q.; Liu, X.; Wong, D. K. *Anal. Chem.* **2013**, *85*, 4350-4356.
(25) Takada, T.; Tochi, T.; Nakamura, M.; Yamana, K. *Bioorg. Med. Chem. Lett.* **2014**, *24*, 2661-2663.
(26) Zhang, Y.; Wang, Y.; Wang, H.; Jiang, J.-H.; Shen, G.-L.; Yu, R.-Q.; Li, J. *Anal. Chem.* **2009**, *81*, 1982-1987.
(27) Abbaspour, A.; Noori, A. *Analyst* **2012**, *137*, 1860-1865.
(28) Castaneda, M. T.; Merkoci, A.; Pumera, M.; Alegret, S. *Biosens. Bioelectron.* **2007**, *22*, 1961-1967.

(29) Yola, M. L.; Eren, T.; Atar, N. *Electrochim. Acta* **2014**, *443*, 117-123.
(30) Rasheed, P. A.; Sandhyarani, N. *Sens. Actuators, B* **2014**, *204*, 777-782.
(31) Fackenthal, J. D.; Olopade, O. I. *Nat. Rev. Cancer* **2007**, *7*, 937-948.
(32) Bonanni, A.; Ambrosi, A.; Pumera, M. *Chem. Eur. J.* **2012**, *18*, 1668-1673.
(33) Liu, B.; Hu, J.; Foord, J. S. *Electrochem. Commun.* **2012**, *19*, 46-49.
(34) Bonanni, A.; Pumera, M. *ACS Nano* **2011**, *5*, 2356-2361.
(35) Ma, W.; Lv, X.; Han, D.; Li, F.; Dong, X.; Niu, L. *J. Electroanal. Chem.* **2013**, *690*, 111-116.
(36) Liu, G.; Luais, E.; Gooding, J. J. *Langmuir* **2011**, *27*, 4176-4183.
(37) Hao, R.-Z.; Song, H.-B.; Zuo, G.-M.; Yang, R.-F.; Wei, H.-P.; Wang, D.-B.; Cui, Z.-Q.; Zhang, Z.; Cheng, Z.-X.; Zhang, X.-E. *Biosens. Bioelectron.* **2011**, *26*, 3398-3404.
(38) Novoselov, K. S.; Geim, A. K.; Morozov, S.; Jiang, D.; Zhang, Y.; Dubonos, S.; Grigorieva, I.; Firsov, A. *Science* **2004**, *306*, 666-669.
(39) Ambrosi, A.; Bonanni, A.; Sofer, Z.; Cross, J. S.; Pumera, M. *Chem. Eur. J.* **2011**, *17*, 10763-10770.
(40) Pumera, M. *Energy Environ. Sci.* **2011**, *4*, 668-674.
(41) Offeman, R.; Hummers, W. *J. Am. Chem. Soc.* **1958**, *80*, 1339-1339.
(42) Staudenmaier, L. *Ber. Dtsch. Chem. Ges.* **1898**, *31*, 1481-1487.
(43) Hong, W.; Bai, H.; Xu, Y.; Yao, Z.; Gu, Z.; Shi, G. *J. Phys. Chem. C* **2010**, *114*, 1822-1826.
(44) Han, X.; Fang, X.; Shi, A.; Wang, J.; Zhang, Y. *Anal. Biochem.* **2013**, *443*, 117-123.
(45) Lee, H.; Tran, M.-H.; Jeong, H. K.; Han, J.; Jang, S.-H.; Lee, C. *Anal. Biochem.* **2014**, *451*, 31-34.
(46) Yao, Y.-J.; Lin, K.-C. *Anal. Chim. Acta* **2014**, *820*, 1-8.
(47) Liu, X.; Wong, D. K. *Talanta* **2009**, *77*, 1437-1443.
(48) Kirubha, E.; Palanisamy, P. *J. Nanosci. Nanotechnol.* **2013**, *13*, 2289-2294.
(49) Revenga-Parra, M.; García-Mendiola, T.; González-Costas, J.; González-Romero, E.; Marín, A. G.; Pau, J.; Pariente, F.; Lorenzo, E. *Anal. Chim. Acta* **2014**, *813*, 41-47.
(50) Li, F.; Peng, J.; Wang, J.; Tang, H.; Tan, L.; Xie, Q.; Yao, S. *Biosens. Bioelectron.* **2014**, *54*, 158-164.
(51) Gao, H.; Sun, M.; Lin, C.; Wang, S. *Electroanalysis* **2012**, *24*, 2283-2290.
(52) Kang, Z.; Yan, X.; Zhang, Y.; Pan, J.; Shi, J.; Zhang, X.; Liu, Y.; Choi, J. H.; Porterfield, D. M. *ACS Appl. Mater. Interfaces* **2014**, *6*, 3784-3789.
(53) Zhao, X.; Pan, F.; Coffey, P.; Lu, J. R. *Langmuir* **2008**, *24*, 13556-13564.
(54) Gao, Z.; Ting, B. P. *Analyst* **2009**, *134*, 952-957.
(55) Carrara, S.; Benini, L.; Bhalla, V.; Stagni, C.; Ferretti, A.; Cavallini, A.; Riccò, B.; Samorì, B. *Biosens. Bioelectron.* **2009**, *24*, 3425-3429.
(56) Mese, F.; Congur, G.; Erdem, A. *J. Electroanal. Chem.* **2014**, *719*, 92-97.
(57) Lazerges, M.; Bedioui, F. *Anal. Bioanal. Chem.* **2013**, *405*, 3705-3714.
(58) Le Floch, F.; Ho, H. A.; Harding-Lepage, P.; Bédard, M.; Neagu-Plesu, R.; Leclerc, M. *Adv. Mater.* **2005**, *17*, 1251-1254.
(59) Uliana, C. V.; Tognolli, J. O.; Yamanaka, H. *Electroanalysis* **2011**, *23*, 2607-2615.
(60) Liang, R.-P.; Xiang, C.-Y.; Zhao, H.-F.; Qiu, J.-D. *Anal. Chim. Acta* **2014**, *812*, 33-40.
(61) Wu, D.; Yin, B.-C.; Ye, B.-C. *Biosens. Bioelectron.* **2011**, *28*, 232-238.
(62) Chen, P.; McCreery, R. L. *Anal. Chem.* **1996**, *68*, 3958-3965.
(63) Zang, Y.; Lei, J.; Hao, Q.; Ju, H. *ACS Appl. Mater. Interfaces* **2014**, *6*, 15991-15997.
(64) Liu, S.; Lin, Q.; Zhang, X.; He, X.; Xing, X.; Lian, W.; Li, J.; Cui, M.; Huang, J. *Sens. Actuators, B* **2012**, *166*, 562-568.
(65) Paredes, J.; Villar-Rodil, S.; Martinez-Alonso, A.; Tascon, J. *Langmuir* **2008**, *24*, 10560-10564.
(66) Frens, G. *Nature* **1973**, *241*, 20-22.

(67) Wang, J. *Analytical Electrochemistry*, 3rd ed.; John Wiley & Sons: United States of America, 2006.
(68) Zhu, C.; Yang, L.; Li, D.; Zhang, Q.; Dou, J.; Wang, D. *Inorg. Chim. Acta* **2011**, *375*, 150-157.
(69) Kim, D. Y.; Yang, J. C.; Kim, H. W.; Swain, G. M. *Electrochim. Acta* **2013**, *94*, 49-56.
(70) Marcano, D. C.; Kosynkin, D. V.; Berlin, J. M.; Sinitskii, A.; Sun, Z.; Slesarev, A.; Alemany, L. B.; Lu, W.; Tour, J. M. *ACS Nano* **2010**, *4*, 4806-4814.
(71) Guo, H.-L.; Wang, X.-F.; Qian, Q.-Y.; Wang, F.-B.; Xia, X.-H. *ACS Nano* **2009**, *3*, 2653-2659.
(72) McCreery, R. L.; Wu, J.; Kalakodimi, R. P. *Phys. Chem. Chem. Phys.* **2006**, *8*, 2572-2590.
(73) Tasca, F.; Harreither, W.; Ludwig, R.; Gooding, J. J.; Gorton, L. *Anal. Chem.* **2011**, *83*, 3042-3049.
(74) Chen, B.; Flatt, A. K.; Jian, H.; Hudson, J. L.; Tour, J. M. *Chem. Mater.* **2005**, *17*, 4832-4836.
(75) Lawson, J.; Erjavec, J. *Modern Statistics for Engineering and Quality Improvement*, 1st ed.; Duxbury Press: United States of America, 2000.
(76) Delaney, J. L.; Doeven, E. H.; Harsant, A. J.; Hogan, C. F. *Anal. Chim. Acta* **2013**, *790*, 56-60.
(77) Yang, W.; Butler, J. E.; Russell, J. N.; Hamers, R. J. *Langmuir* **2004**, *20*, 6778-6787.
(78) Nimmagadda, R. D.; McRae, C. *Tetrahedron Lett.* **2006**, *47*, 5755-5758.
(79) Ravera, M.; Bagni, G.; Mascini, M.; Osella, D. *Bioinorg. Chem. Appl.* **2007**, *2007*, 1-11.

Chapter 6

SUPPLEMENTARY MATERIAL

6.1 Supplementary material

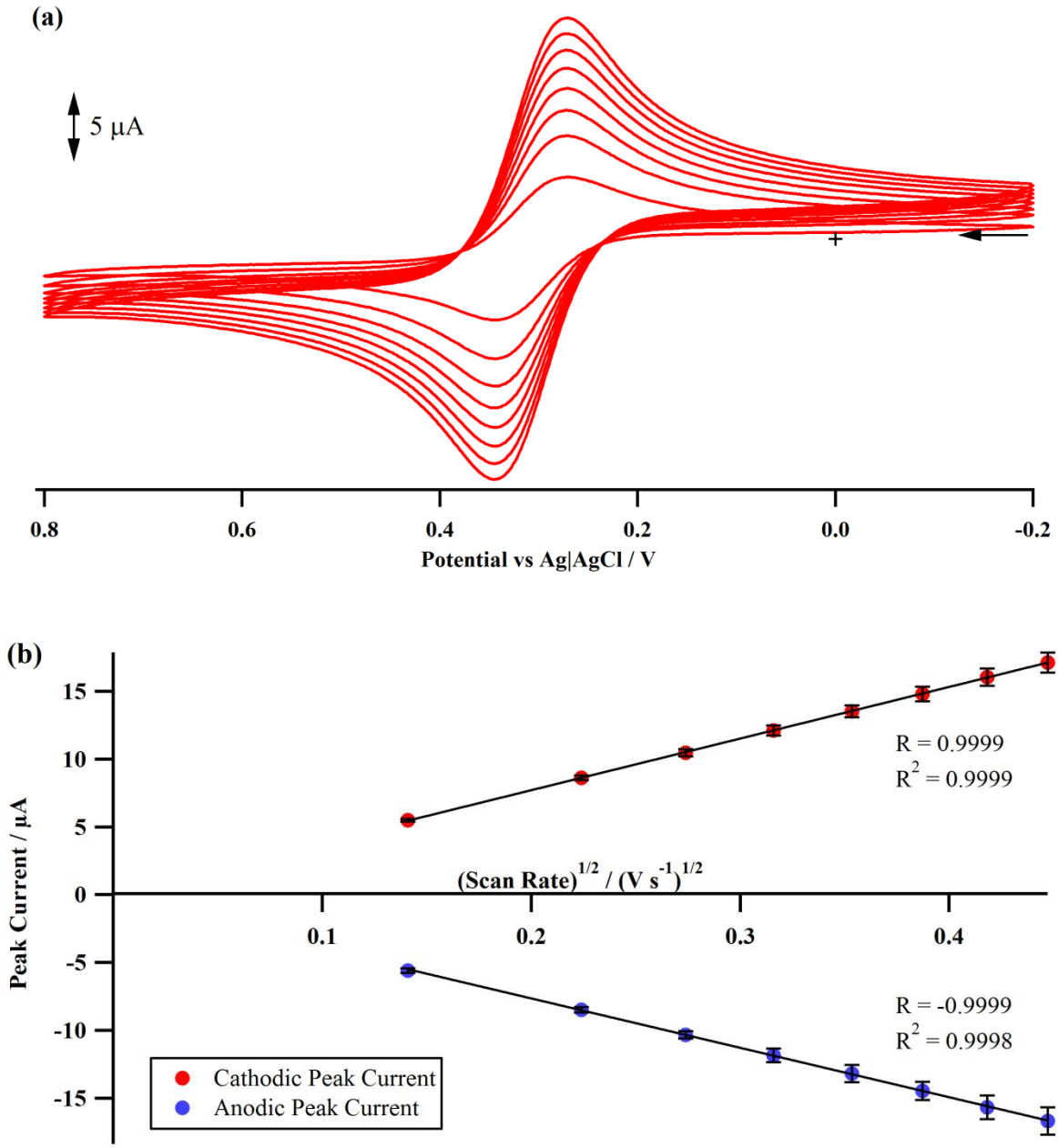

Figure 6.1 (a) Cyclic voltammetry of 1 mM ferrocenecarboxylic acid in pH 7.4 PBS at a polished glassy carbon electrode at different scan rates, the third scan of each scan rate is shown in this figure. (b) A plot of cathodic and anodic peak current versus (scan rate)$^{1/2}$. Error bars depict 95% confidence intervals.

Table 6.1 A full 2^3 factorial design to identify significant effects and interactions. Oxidation peak current of 1 mM ferrocenecarboxylic acid in pH 7.4 PBS was used as the response signal.

Run	X_1	X_2	X_3	X_1X_2	X_1X_3	X_2X_3	$X_1X_2X_3$	Run Order	$I_{oxidation}$ / μA	Mean / μA	Variance (s^2)
1	-	-	-	+	+	+	-	12, 15	11.7, 13.5	12.6	1.6
2	+	-	-	-	-	+	+	1, 5	14.5, 8.6	11.6	17.1
3	-	+	-	-	+	-	+	7, 8	12.4, 12.3	12.3	0.0
4	+	+	-	+	-	-	-	9, 6	14.9, 10.6	12.7	9.4
5	-	-	+	+	-	-	+	14, 10	11.5, 11.0	11.2	0.1
6	+	-	+	-	+	-	-	13, 2	13.8, 12.5	13.2	0.8
7	-	+	+	-	-	+	-	11, 3	9.6, 11.4	10.5	1.7
8	+	+	+	+	+	+	+	16, 4	10.5, 10.2	10.3	0.0
Sum product	1.21	-2.61	-3.90	-0.750	2.38	-4.48	-3.54				
Effect	0.303	-0.653	-0.975	-0.188	0.595	-1.12	-0.885				
t_E	0.308	-0.665	-0.993	-0.191	0.606	-1.14	-0.901		t*(8 degrees of freedom) = 2.31		

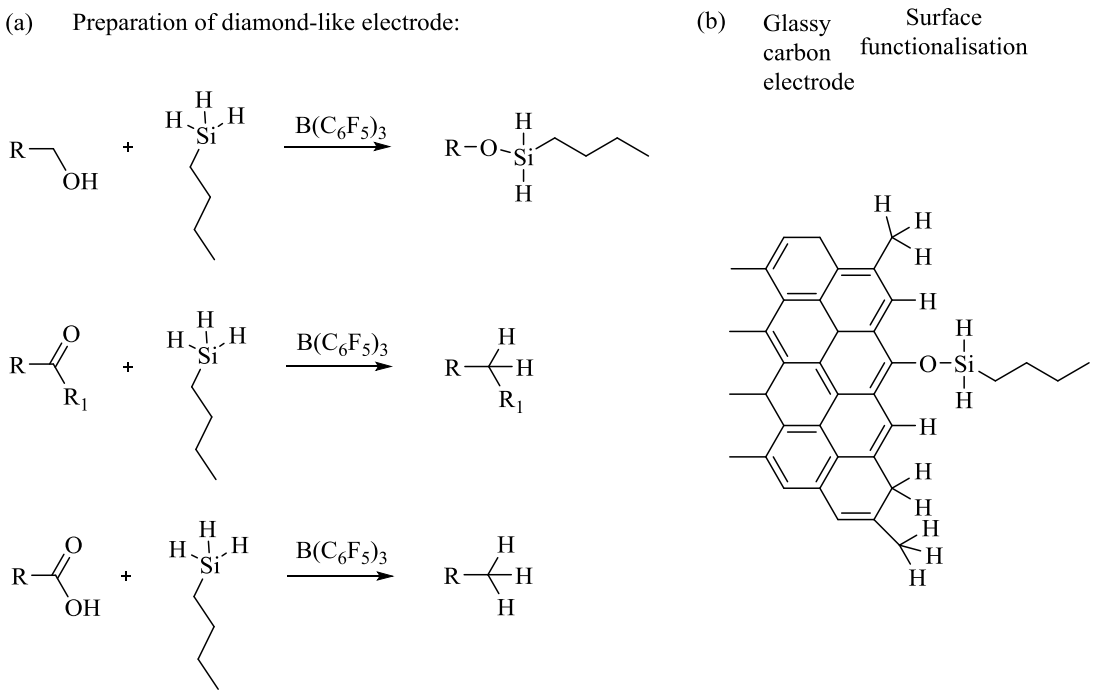

Figure 6.2 (a) Reduction reactions of primary alcohols, ketones and carboxylic acids using silane-based reduction with n-butylsilane, catalysed with the Lewis acid tris(pentafluorophenyl)borane, to form the corresponding alkanes and silyl ethers, where R = phenyl and R_1 = alkyl, aryl or H. (b) Potential surface groups present on a glassy carbon electrode following silane reduction of oxygen-containing functional groups using silane-based reduction.

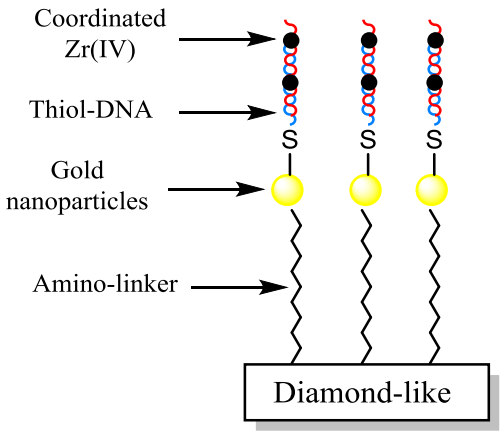

Figure 6.3 Overall design of the proposed diamond-like electrochemical DNA biosensor.